Hypoxic stress dysregulates functions of glioma-associated myeloid cells through epigenomic and transcriptional programs

Monika Dzwigonska[1], Patrycja Rosa[1], Beata Kaza[1], Salwador Cyranowski[1], Aleksandra Ellert-Miklaszewska[1], Agata Kominek[2], Tomasz Obrebski[3], Anna R. Malik[3], Katarzyna Piwocka[2], Jakub Mieczkowski[4], Bozena Kaminska[1#] and Katarzyna B. Leszczynska[1,#]

[1] Laboratory of Molecular Neurobiology, Nencki Institute of Experimental Biology, Warsaw, Poland;

[2] Laboratory of Cytometry, Nencki Institute of Experimental Biology Polish Academy of Sciences, 02-093 Warsaw, Poland

[3] Cellular Neurobiology Research Group, Institute of Developmental Biology and Biomedical Sciences, Faculty of Biology, University of Warsaw, Miecznikowa St. 1, Warsaw 02-096, Poland

[4] 3P-Medicine Laboratory, Medical University of Gdansk, Gdansk, Poland

[#] correspondence: k.leszczynska@nencki.edu.pl; b.kaminska@nencki.edu.pl

ORCID:

KBL - 0000-0002-3504-1553
MD - 0000-0003-1774-3671
BK - 0000-0002-2642-4616
JM - 0000-0002-2091-012X
ARM - 0000-0001-7732-0756
TO - 0000-0001-8137-8774
KP - 0000-0001-6676-5282
AK - 0000-0003-1567-9442
AEM - 0000-0002-7947-5660
SC - 0000-0001-9611-531X
BK (Kaza) - 0000-0002-3630-6496

KEYWORDS: tumour-associated myeloid cells, glioma, microglia, macrophages, hypoxia, epigenetics, chromatin accessibility

ABSTRACT

Hypoxia rapidly alters gene expression to allow cellular adaptation to challenging conditions and support tumour growth. Hypoxia also affects the chromatin structure by modifications of histones and DNA methylation. Glioblastoma (GBM) is an aggressive, deadly primary brain tumour for which there is no effective treatment. The tumour microenvironment of GBM is highly heterogeneous, with infiltration of glioma-associated microglia and macrophages (GAMs) and the presence of necrotic, hypoxic regions. The mechanisms through which hypoxia alters the tumour microenvironment and regulates functions of infiltrating immune cells remain poorly understood.

Here, we show that hypoxia modulates the expression of myeloid markers in distinct ways: upregulates the monocytic marker *Lgals3* expression and downregulates the microglial markers *P2ry12* and *Tmem119* in microglial and monocytic GAMs *in vitro* and *in vivo*, as shown using human and mouse GBM single-cell transcriptomics datasets. The genome-wide hypoxia-dependent transcriptomic changes in microglial cells were determined in microglia-glioma co-cultures. Numerous GAM subtype markers were dysregulated in response to hypoxic stress due to associated changes in chromatin accessibility, as determined using ATACseq. While hypoxia alone drives a decrease of the overall chromatin accessibility at gene promoters, the exposure to glioma cells under hypoxic conditions leads to both increases and decreases of chromatin accessibility at promoter regions in microglial cells. Hypoxia downregulates the chromatin accessibility at the regions enriched in motifs of transcription factors regarded as master regulators of microglial cell identity and function, including *SPI1* or *IRF8*. Overall, our data highlights the importance of hypoxic stress as a strong intratumoral regulator of myeloid cell functions, which adds complexity to the characterisation of particular GAMs subpopulations.

INTRODUCTION

Glioblastoma (GBM) is the most aggressive primary brain tumour, incurable with existing therapies (1). The highly heterogeneous tumour microenvironment (TME) of GBM significantly contributes to the complexity and malignancy of these tumours (2). Myeloid cells recruited to the tumour, including brain-resident microglia and bone marrow-derived monocytes and macrophages (BMDMs), collectively known as tumour- or glioma-associated microglia/macrophages/monocytes (TAMs/GAMs), constitute up to 30% of the GBM mass (3,4). Recent applications of single-cell transcriptomics characterised GAM subpopulations in human GBMs and experimental gliomas, revealing a heterogeneity of myeloid cells (5–12). The two major groups: microglia-GAMs (Mg-GAMs) and monocytic/macrophage GAMs (Mo/Mφ -GAMs) were further stratified into specialised subpopulations with predominant phenotypes: homeostatic, interferon, chemotactic, phagocytic, lipid, ribosomal, hypoxic, proliferative or transitory phenotypes (5–8,12,13). These subpopulations of GAMs have specific gene expression patterns, which are often used to select the characteristic markers for each GAM subtype. Despite some functional specialisation, most GAM subpopulations actively support tumour progression and immunosuppression (3,14).

Advances in spatial transcriptomics showed that the proportions of Mg-GAMs and Mo/Mφ-GAMs are different in certain tumour areas, with an indication that a higher proportion of Mo/Mφ-GAMs is found at the tumour core, potentially due to an influx of BMDMs through leaky, disorganised tumour vasculature at the later tumour stages (7,8,10,15). Mg-GAMs, on the other hand, are more enriched at the tumour periphery, tumour border and the surrounding brain parenchyma (5,6,14). While in the tumour core, GAMs can be exposed to hypoxic stress (shortage of oxygen), which leads to rapid gene expression changes that allows adaptation to challenging oxygen-deprived conditions (16,17). However, the role of hypoxia in GAMs is only starting to emerge. Some studies showed that while in hypoxia, GAMs acquire

immunosuppressive and immunotolerant phenotypes (14) or can increase the permeability of GBM vasculature through the release of adrenomedullin (8). Pre-clinical testing demonstrated that targeting adrenomedullin in GBM is a good strategy to improve blood vessel normalisation and drug delivery (8). A recently discovered new subtype of GAMs, "lipid-laden TAMs", were found to reside in hypoxic niches and use myelin-derived lipids to fuel the aggressiveness of glioma cells (11). Altogether, these findings emphasize the importance of hypoxic stress in shaping distinct GAM phenotypes in GBM. However, it remains unclear if and how hypoxia can shift GAM subpopulations into particular states and phenotypes.

Single-cell transcriptomics data defined the sets of genes that are characteristic for particular Mo/Mφ-GAM and Mg-GAM sub-clusters (5–8,12). However, some myeloid markers, which are highly expressed across multiple subtypes of GAMs, are affected by various environmental cues, which raises the awareness of whether selective GAM markers can detect a particular GAM subpopulation, e.g. in immunohistology. For example, *LGALS3,* the gene encoding galectin-3 (GAL3) is often used as a general monocytic and macrophage GAM marker distinguishing the Mo/Mφ-GAMs from Mg-GAMs (5,8). However, *LGALS3* is also highly expressed in more specialised lipid Mo/Mφ-GAMs due to its function in lipid processing and accumulation (6,8). In addition, some studies showed that *LGALS3* is hypoxia-inducible in a number of cell types, including cancer cells (18,19). Therefore, we hypothesised that *LGALS3,* and potentially some other myeloid subtype markers, could be altered by hypoxic stress either in Mg-GAMs or in Mo/Mφ-GAMs, which in turn could affect the revealing of the spatial distribution of various GAM subpopulations. The mechanisms underpinning transcriptomic changes driven by hypoxic stress in GAMs are poorly defined. Here, we showed that along with known hypoxia-regulated genes *Vegfa* and *Glut1* (20,21), hypoxia upregulates the monocytic/macrophage marker *Lgals3* expression and downregulates the microglial markers *P2ry12* or *Tmem119*, both in microglial and macrophage cells. We find similar correlations

between the hypoxic score and gene expression *in vivo* in human and mouse GBM single-cell transcriptomics datasets. Using direct microglia-glioma co-culture we defined genome-wide hypoxia-dependent transcriptomic changes in microglial cells. We found that numerous GAM subtype markers were dysregulated in response to hypoxic stress, and these changes were associated with epigenomic alterations detected with ATACseq. While hypoxia alone decreases the overall chromatin accessibility at gene promoters, contacts with glioma cells under hypoxic conditions lead to far more extensive remodelling of chromatin accessibility at promoter regions in microglial cells. Our data highlights hypoxic stress as a strong intratumoral regulator of myeloid subtype gene expression by imposing epigenomic and transcriptomic changes.

RESULTS

Hypoxia dysregulates expression of *Lgals3*, *P2ry12* and *Tmem119* in myeloid cells *in vitro* and in GAMs *in vivo*

We investigated whether hypoxia directly alters *Lgals3* expression in various macrophage and microglial cells using mouse microglial BV2 cells, RAW 264.7 cells (a tumour-derived mouse macrophage cell line) and primary mouse bone marrow-derived macrophages (BMDM). In three cell types, hypoxic conditions (<0.1% O_2) led to upregulation of *Lgals3* expression at the mRNA and protein levels, along with known hypoxia-induced genes *Vegfa* and *Glut1* (**Figure 1A-B**). *Lgals3* expression was also modulated in response to a milder hypoxia (1% O_2) and a hypoxia-mimetic drug ($CoCl_2$), which inhibits the activity of prolyl hydroxylases and therefore leads to HIF-α stabilisation in normoxic conditions (22). Both the mild hypoxia and $CoCl_2$ upregulated the expression of *Lgals3* at the mRNA and protein levels (**Supplementary Figure 1A-B**). Interestingly, under the same conditions, the expression of microglial markers *Tmem119* and *P2ry12* was significantly downregulated. While *Tmem119* and *P2ry12* are microglia

markers, their expression was detected in RAW 264.7 and BMDM cells, and was downregulated by hypoxia (**Figure 1C**). Moreover, the mild hypoxia and $CoCl_2$ also decreased the expression of these genes (**Supplementary Figure 1C**). Overall, this data suggest that hypoxic stress regulates the expression of *Lgals3* and *Tmem119* and *P2ry12* in opposite directions, irrespective of the origin of the affected myeloid cell.

We verified the expression of these genes in mouse GBM GAMs in relation to hypoxia *in vivo,* by exploring the public scRNAseq dataset from Antunes at al., which has annotations of multiple GAM sub-clusters, including microglia, monocytes, lipid, proliferative, IFN, but also hypoxic clusters (related as tumour-associated microglia (Mg-TAMs) and tumour-associated monocytes/macrophages (Mo-TAMs)) (6). The published annotation of clusters in this dataset shows that cells in the hypoxic cluster (**Figure 1D**) have high *Lgal3* expression, and that hypoxic cells are mostly assigned to the Mo-TAMs clusters rather than to the Mg-TAMs (**Figure 1D-F**). We extracted the top genes expressed in hypoxic GBM TAMs cluster from another scRNAseq dataset (8) and created a combined "hypoxia score", which encompasses common top hypoxia TAM cluster genes from both studies (**Supplementary Table S1**). When the expression of combined "hypoxia score" was analysed in the scRNAseq Antunes-dataset, in addition to the initial hypoxic Mo-TAMs cluster (**Figure 1D**), some groups of hypoxic cells were also visible in other clusters of TAMs, particularly in the lipid Mo-TAMs, transitory Mo-TAMs, proliferative Mo-TAMs and in Mg-TAMs (**Figure 1E**). In agreement with the literature, *Lgals3* expression was stronger in the whole Mo-TAM subpopulation in comparison to Mg-TAMs (5), however, it was further upregulated in TAMs with increased "hypoxia score" in proliferative, lipid, monocytic and transitory Mo-TAMs (**Figure 1F**). The expression of *Tmem119* and *P2ry12* was higher in Mg-TAMs than in Mo-TAMs, however, it decreased in Mg-TAMs along with increased "hypoxia score" (**Figure 1G-H**). Gene expression shows a statistically significant positive correlation of the "hypoxia score" with *Lgals3* and a negative

correlation with *Tmem119* and *P2ry12* across all TAMs and specifically in Mg-TAMs (**Figure 1I**). Importantly, these observations were confirmed in the human newly-diagnosed and recurrent GBM TAM Antunes datasets (**Figure 1I** and **Supplementary Figure 2**) (6).

To corroborate these findings further, we analysed the human GBM samples from the IvyGAP glioblastoma project, where the gene expression was tested in samples microdissected from the distinct spatial locations in GBM biopsies, including perinecrotic regions known to be hypoxic, vascularised areas, tumour leading edge, infiltrative tumour or cellular tumour (23). The expression of *LGALS3* was the highest in the perinecrotic and pseudopalisading regions (CTpnz and CTpcan) in a similar way as the expression of some typical hypoxic markers such as *CA9*, *SLC2A1* or *VEGFA* (**Figure 1J**). On the contrary, the expression of *TMEM119* and *P2RY12* was the lowest at the hypoxic perinecrotic and pseudopalisading areas and the most abundant in the infiltrating tumour (IT) and tumour leading edge (LE) (**Figure 1J)**. While it may reflect the fact that *TMEM119* or *P2RY12* expressing cells are less abundant in the perinecrotic regions, this data also suggest that hypoxia strongly dysregulated the expression of the tested genes in tumours *in vivo*, irrespectively of the cell types exposed to hypoxic stress.

Reprograming of the transcriptome of BV2 microglial cells by glioma and hypoxia

To better understand the role of hypoxia in controlling the gene expression in myeloid cells associated with the tumour, we have employed direct BV2 microglia-glioma co-cultures (**Figure 2A**), which recapitulate tumour-microglia interactions during tumour progression (24). Glioma cells (GL261-GFP) were seeded in culture dishes and the BV2 microglial cells were added the next day. After 24 h BV2-GL261 co-culture was either transferred into hypoxic conditions (<0.1% O_2) or left in normoxia (21% O_2) for additional 16 hours. (**Figure 2B**). BV2 cells without co-culture with glioma cells served as controls. After the hypoxic treatment, the co-cultures were dissociated into single-cell suspensions, and BV2 cells immuno-labelled with

anti-CD45-PE antibody were separated from glioma cells by FACS sorting, which allowed us to obtain pure populations of cells (**Supplementary Figure 3A-B**). To avoid any reoxygenation-dependent gene expression changes that could occur during cell staining and FACS procedure, the co-cultures were fixed with a glyoxal fixative straight after hypoxic treatment and RNAseq of sorted CD45+ BV2 cells was performed. The glyoxal fixation was recently validated as suitable for the downstream RNAseq analysis (25). We confirmed the high RNA quality of glyoxal-fixed samples, and induction of hypoxia-dependent genes by qPCR (**Supplementary Figure 3C-D**). Moreover, we observed morphological changes in BV2 microglial cells co-cultured with glioma cells, characterised by more elongated shapes in hypoxic conditions (**Figure 2B**).

The principal component (PC) analysis of the BV2 RNAseq data showed a clear separation between all four conditions tested: BV2 cells isolated from normoxic co-cultures with glioma (CC_N), BV2 cells isolated from hypoxic co-cultures with glioma (CC_H), BV2 monocultures in normoxia (CTRL_N) and BV2 monocultures in hypoxia (CTRL_H) (**Figure 2C**). A stronger separation of samples was observed due to hypoxic stress (samples separating along the PC1 axis) as opposed to the co-culture effect (samples separating along the PC2 axis). Differential gene expression analysis showed that co-culture of BV2 cells with glioma cells induced expression of 412 genes and decreased 44 genes (CC_N versus CTRL_N; threshold at $\log_2 FC = 1$ and p-value < 0.05; **Supplementary Figure 4A**). Exposure of BV2-GL261 co-cultures to hypoxia induced many more transcriptomic changes in BV2 cells, with 2605 upregulated and 1942 downregulated genes (CC_H versus CC_N; **Supplementary Figure 4B**). Hypoxia alone also induced a large number of transcriptomic changes in BV2 cells (1786 up and 2267 down; CTRL_H versus CTRL_N) (**Suplementary Figure 4C**), of which the majority overlapped with the gene expression changes induced by hypoxia in co-cultures (**Figure 2D-E**). Interestingly, genes that were up- or downregulated by hypoxia (either in co-cultures or alone) had a much

higher mean basal expression than the genes that were altered in response to the contacts with glioma alone in normoxic conditions (**Supplementary Figure 4D-F**).

We confirmed that BV2 cells in monoculture or in co-culture with glioma cells showed upregulation of HIF activity upon exposure to hypoxia by measuring the expression of genes from the validated specific HIF score (26). The HIF score gene expression was significantly increased under hypoxic conditions (**Supplementary Figure 4G**). Moreover, the analysis of promoters of the upregulated genes showed the enrichment in the motifs of transcription factors (TF) that are typical for the hypoxic response, including HIF-1α, HIF-2α, KLFs, ATF3 or ATF4 (**Supplementary Figure 4H**) (26–30). Overrepresentation analysis (ORA) of Gene Ontology (GO) terms using genes upregulated in glioma-co-cultured BV2 cells exposed to hypoxia showed the enrichment of the processes typical for hypoxia, including response to decreased oxygen levels, angiogenesis, blood vessels morphogenesis, chemotaxis or cell motility-related processes (**Figure 2F** and **Supplementary Table S2**). Interestingly, the upregulation of pathways related to axon development, axon guidance or tissue morphogenesis in BV2 microglial cells indicated a strong shift towards the changes in cell morphology (**Figure 2F**), which was in line with our observations from immunofluorescent analysis of the BV2 cell morphology in hypoxic co-culture (**Figure 2B**). The downregulated genes in BV2 cells from glioma co-cultures under hypoxia were associated with the pathways previously reported as repressed in hypoxia, including ribosomal biogenesis, RNA processing or DNA replication (**Figure 2G**) (31,32).

Further analysis of genes induced or decreased more significantly in the presence of hypoxia and glioma co-culture as opposed to the hypoxia alone, indicated processes related to axonogenesis, axon development and other morphological changes (**Figure 2H** and **Figure 2I**, right panel includes examples of genes from the axon development pathway; see **Supplementary Table S2** for the full list). Interestingly, the genes more decreased by hypoxia

and co-culture with glioma cells in comparison to hypoxia alone included genes from the pathways related to leukocyte or myeloid cell differentiation, including *Mef2c, Tnfrsf11a, Rassf2, Lfng, Slc9b2, Nfam1, Ighm* or *Dyrk3* (**Figure 2I**, left panel) and **Supplementary Table S2**). This finding supports the hypothesis that hypoxia potentially influences the expression of myeloid marker genes in GAMs, but also that hypoxia *in vivo* additionally imposes the gene expression changes driven by interactions of GAMs with glioma cells.

Hypoxia dysregulates the expression of multiple Mo/Mφ and microglial marker genes

Based on the published scRNAseq data reports, which distinguished particular Mg-GAMs and Mo-GAMs populations, as well as further subpopulations of Mo/Mφ -GAMs characterised as transitory, IFN, lipid, hypoxic, chemotactic, phagocytic, ribosomal or proliferative, we have created a list of genes highly expressed in distinct GAM clusters across multiple studies (**Supplementary Table S3**) (5–8). We then investigated the expression of these genes in hypoxic BV2 cell monocultures (Hyp) or BV2 co-cultures with glioma cells under normoxic (CC) or hypoxic conditions (CC+Hyp). Firstly, we found that most of the genes selected from the hypoxic-GAMs clusters (high "hypoxia score") were upregulated by hypoxia in BV2 cells (**Figure 3A**). Secondly, numerous genes defining specific clusters were also significantly affected by hypoxia in BV2 cells, including myeloid markers common for Mg-GAMs and Mo/Mφ-GAMs (**Figure 3B**). Furthermore, we found that markers of IFN, Transitory and Ribo-GAMs were predominantly downregulated by hypoxia, while phagocytic and chemotactic GAMs genes were induced by hypoxia in BV2 cells (**Figure 3C**). These findings are in agreement with previous reports, showing that ribosomal and RNA processing genes are downregulated in response to hypoxia (31,33). On the other hand, the chemotaxis and phagocytic phenotype genes upregulated in response to hypoxia suggest the active rearrangements in the cytoskeleton and increased motility of these myeloid cells facilitating cell migration and clearing of the necrotic debris (3,8). The genes from the lipid-GAMs cluster were

mostly upregulated in hypoxic co-cultures, including *F10, Lgals3, Gpnmb, Apoe* or *Ctsb* (**Figure 3C**). However, some markers such as *Ftl1, Fth1* or *Fabp5* were found significantly downregulated, suggesting that the overall role of hypoxia in driving the lipid phenotype in TAMs is complex (**Figure 3C**). In many cases, the hypoxia in the BV2-glioma co-culture had a similar effect on the expression of the tested markers as hypoxia alone, although for some single genes, the differences were noted (**Figure 3B-C**).

To dissect regulatory networks, we search for the top TF motifs that were enriched at the promoters of hypoxia-upregulated or downregulated myeloid marker genes analysed here. In addition to the enriched HIF-1/2A binding sites, other TF motifs were also detected in hypoxia-increased genes, including those for MAX, RUNX, NF-κB, AP1 and others (**Figure 3D**). Motifs for ISRE, BCL6 and ETV1 were found as enriched in the promoters of hypoxia-downregulated genes (**Figure 3D**). Overall, the results indicate that hypoxia has a dominant effect on the expression of numerous GAMs markers, which in turn may affect the function of particular myeloid cells present within the TME, with a potential role in supporting tumorigenesis.

To study whether hypoxia-reprogrammed myeloid cells support glioma aggressiveness, we performed an RNAseq analysis on GL261 glioma cells from monocultures and co-cultured with BV2 cells (**Figure 4A**). The PCA analysis showed a very strong effect of hypoxia on sample separation either in co-culture or GL261 alone (**Figure 4B**) and numerous transcriptomic changes in GL261 cells in response to hypoxia in co-culture with BV2 or to hypoxia alone were noted (**Figure 4C-E**). Overall, the hypoxic stress induced a typical hypoxia response in both cases, as determined with the ORA GO analysis (upregulation of processes related to decreased oxygen levels, angiogenesis, etc.; **Figure 4F-G**). However, the most significantly enriched process within upregulated genes for glioma co-cultures under hypoxia was positive regulation of locomotion, cell migration and motility, while for hypoxic GL261 monocultures the top

enriched pathways included fat cell differentiation and response to oxygen levels (**Figure 4F and G**, respectively and **Supplementary Table S4**). These results indicate that the presence of microglial cells under hypoxic conditions enhanced the migratory and invasive phenotype of glioma cells, which is in line with the more aggressive phenotype observed in patients with hypoxic tumours.

Glioma and hypoxia exposure reprograms the epigenome of BV2 cells

It was previously shown that hypoxia can significantly alter the chromatin landscape in cancer cells (31,34–36). Therefore we considered hypoxia-induced chromatin remodelling as a causative factor for differential gene expression in microglia. First, we performed an immunofluorescent (IF) staining of key histone modifications to verify whether hypoxia affects these marks in microglia co-cultured with glioma cells. As shown, hypoxia globally increased H3K27me3 or H3K9me3 marks both in glioma and in BV2 cells (**Supplementary Figure 5A-D**). This prompted us to investigate the chromatin accessibility patterns in glioma-interacting microglia cells in normoxic and hypoxic conditions using ATACseq assay (**Supplementary Figure 5E**). To prevent any reoxygenation-dependent chromatin changes, we have performed an ATACseq assay on cells fixed with formaldehyde prior to the separation of co-cultures with flow cytometry and further processing (34). Overall, we have detected 26718 ATACseq peaks across all conditions, of which 0.1% were specific to CTRL_N, 6.5% specific to CC_N, 14.5% specific to CTRL_H and 11.3% specific to CC_H (**Supplementary Figure 5F**). Interestingly, the PCA analysis on ATACseq peaks showed that co-culture with glioma cells had a much stronger effect on the chromatin accessibility in BV2 cells (separation along the PC1 axis) than hypoxia (separation along the PC2 axis) (**Figure 5A)**. The co-culture of BV2 with glioma cells in normoxia resulted in a larger number of differentially increased than decreased chromatin accessibility peaks in BV2 cells (2173 up and 716 down peaks, respectively; **Supplementary Figure 5G**). However, the co-culture of BV2 with glioma cells in hypoxia further dysregulated

chromatin accessibility in BV2 cells in comparison to glioma-co-culture in normoxia or to hypoxia-alone (4418 up and 3885 down peaks in hypoxic coculture; 1831 up and 1514 down peaks in hypoxia alone control; **Supplementary Figure 5H-I**). We then analysed the genomic localisation of differentially regulated peaks and found specific differences in the number of promoter-associated and intron-associated peaks in normoxic BV2 co-cultures or in hypoxic BV2 monocultures (differences in up versus down peaks in CC and in Hyp alone; **Figure 5B**). Namely, co-culture in normoxia resulted in the upregulation of promoter and intronic peaks (**Figure 5B**, left panel), while hypoxia alone led to the downregulation of promoter peaks (**Figure 5B**, right panel). Importantly, a combination of these two factors (co-culture in hypoxia) resulted in a relatively similar number of up and downregulated promoter or intron peaks (**Figure 5B**, middle panel). Further analysis of the upregulated peaks, specifically at the promoter regions, showed that 109 peaks out of 1680 CC_Hyp UP peaks (6.49%) were also increased due to hypoxia alone, while 1515 upregulated peaks required specific concomitant exposure to hypoxia and glioma (**Figure 5C**). Amongst the downregulated promoter peaks (**Figure 5D**), 483 (33.56%) out of 1439 CC_Hyp DOWN peaks were also downregulated due to hypoxia alone, and 951 required specific concomitant exposure to hypoxia and glioma for their downregulation. This suggested that hypoxia as a single factor had a stronger impact on the downregulation rather than on the upregulation of promoter region openness (**Figure 5B-D**). In turn, the combined factors of glioma presence and hypoxia were important for gaining accessible promoters in hypoxic BV2 cells.

Further analysis of promoter peaks and genic peaks (including the promoter and gene body) assigned to particular genes showed that the ATACseq peaks allocated solely to the promoters of the HIF-inducible genes were not significantly increased in response to hypoxia (**Figure 5E**). However, including genic peaks in the analysis of the HIF score showed significant upregulation of ATACseq peaks in the HIF score genes in response to hypoxia (and more

significant in control hypoxia samples), suggesting that peaks outside of the promoters were particularly induced in response to hypoxia at the HIF-target genes (**Figure 5F**) (26). This result was additionally confirmed by the TF enrichment analysis on all upregulated ATACseq peaks. HIF-1A and HIF-2A enrichment was only found in genic, but not promoter regions in hypoxic cells from monocultures (**Figure 5G**).

In addition, a number of TFs were enriched at the genic peaks both in co-cultured and control hypoxic cells, including AP1 (FOS and JUN subunits), ATF1-4, FRA1-2, CHOP, and others (**Figure 5G**). TF motifs that were the most specifically and significantly enriched in upregulated peaks in hypoxic co-cultures included the ones that have been implicated in the regulation of microglial cell functions (**Figure 5G**). We found motifs for KLF6 and EGR1, which play a role in the regulation of microglial activation and inflammatory responses (35,36), for KLF4 which is involved in microglial cell polarization and differentiation (37), for KLF9 known to regulate oxidative stress responses in microglia (38), for SP1 involved in microglial cell activation, survival and proliferation (39) and SMAD3 regulating activity, differentiation, and maintaining a quiescent state of microglial cells (40). Similarly as in the RNAseq analysis, the ORA GO analysis at decreased genic ATACseq peaks showed downregulation of processes related to mitotic cell division, GTPase activity, DNA replication and various RNA processing mechanisms (**Figure 5H**). On the contrary, the upregulated genic ATACseq peaks were associated with histone modification, dendrite development, autophagy, vesicle organisation and other processes (**Figure 5I**).

As our data so far suggested that the glioma co-culture factor had the strongest influence on the chromatin accessibility changes in microglia specifically in hypoxic conditions (**Figure 5B**), we verified which peaks and associated processes were the most enriched during glioma co-culture in hypoxia when compared to hypoxic monocultures. Out of 4418 peaks upregulated in co-cultured hypoxic BV2, 2257 peaks were more enhanced in hypoxia co-culture in comparison

to hypoxic BV2 monocultures (**Supplementary Figure 6A**). Out of 3385 downregulated peaks in co-cultured hypoxic BV2, 1638 were more decreased in hypoxia co-culture in comparison to hypoxic BV2 monocultures. The genomic annotation analysis of these peaks suggested that the combined effect of BV2 in hypoxic co-cultures when compared with hypoxia-alone led to an increase in chromatin accessibility at the promoter regions and a decrease in accessible introns and distal intergenic chromatin sites (**Supplementary Figure 6B**). The ORA GO analysis of these enhanced changes in promoters with increased accessibility specifically in co-cultured hypoxic BV2 cells showed upregulation of processes such as autophagy, histone modifications, cellular components disassembly etc (**Supplementary Figure 6C-D**). Interestingly, while there was a low number of genes with the decreased chromatin accessibility at the gene promoters in response to co-culture and hypoxia, these genes were associated with the neuroinflammatory responses, defence responses or microglial cell activation (**Supplementary Figure 6C-D**). This suggests that hypoxia and glioma exposure by reducing chromatin accessibility supports the immunosuppressive phenotype of BV2 cells. In turn, processes associated with the changes at intronic and exon peaks specifically in hypoxic co-cultures were associated with tissue specific differentiation processes and regulation of cellular signalling, including GTPase activity, calcium ion homeostasis, metal ion transport etc in the downregulated peaks, respectively (**Supplementary Figure 6E**).

Concordant hypoxia-dependent transcriptomic and epigenomic changes in glioma-co-cultured BV2 cells impact myeloid cell functional markers

Subsequently, we compared differential changes in the gene expression and chromatin accessibility in the glioma-co-cultured BV2 cells. The Spearman and Pearson correlation coefficients (0.24) for ATACseq peaks and gene expression indicated a partial but significant correlation of affected genes in both datasets (**Figure 6A**). Out of 2605 genes with induced expression, 645 had concordant changes in the chromatin accessibility (24.76%) (**Figure 6B**).

For the 1942 genes with decreased expression, 345 had concordant downregulation of chromatin accessibility in the same condition (17.76%) (**Figure 6C**). The ORA GO analysis on the concordant upregulated genes indicated response to hypoxia as the top pathway, but also other quite diverse biological processes, including regulation of transcription in response to stress, neuron migration, muscle organ development and other (**Supplementary Figure 7A** and **Supplementary Table S5**). The concordant downregulated genes indicated typical processes known to be downregulated in hypoxia, including ribosome biogenesis, DNA replication, cell cycle division etc (**Supplementary Figure 8B** and **Supplemementary Table S5**). Very few of the concordant changes were additionally enhanced in BV2 cells co-cultured with glioma in hypoxia when compared to hypoxia alone (29 genes up and 10 genes down). However, among the genes specifically downregulated in hypoxic co-cultures there were genes falling into significantly enriched GO processes, such as semaphoring-plexin signalling pathway involved in neuron projection guidance, signal release, regulation of secretion by cell, but also again myeloid leukocyte differentiation (**Supplementary Figure 8C** and **Supplementary Table S5**). These processes represent homeostatic functions of microglia (3,5).

The downregulation of the myeloid leukocyte differentiation process in concordant changes brought us to our initial findings that some myeloid markers or GAM cluster genes might be dysregulated in hypoxia through chromatin remodelling. We found that out of 53 transcriptionally induced GAM-associated marker genes (from **Figure 3**), 18 (34%) had concordant changes in the chromatin accessibility in BV2 cells co-cultured with glioma in hypoxic conditions (**Figure 6B,** lower box). Similarly, for the significantly downregulated GAM-associated marker genes, 5 out of 32 (15.6%) were concordantly decreased at the mRNA and chromatin accessibility level (**Figure 6C,** lower box). Of the concordantly dysregulated myeloid cell markers in hypoxia, some were already described as crucial for the tumour-supportive role and lipid metabolism in GAMs or directly in immunosuppression. *Gpnmb* was

recently shown to play an immunosuppressive role in the tumour microenvironment of glioma as its deletion increased the inflammation and reduced the tumour size (41). We have scanned for the presence of specific TF motifs in the upregulated chromatin accessibility peak in the *Gpnmb* promoter and found SMAD2, SMAD4, NFIB and NFIC among the most frequent TF motifs occurring within this peak (**Figure 6D** and **Supplemementary Table S6**). The TGFB/SMAD axis is already known to regulate the immunosuppressive phenotypes in myeloid cells (42). In turn, at the *Lgals3* promoter, the upregulated accessible chromatin region was abundant with binding motifs for AP-1 and ATF3 TFs (**Figure 6E** and **Supplemementary Table S6**), which can mediate the tumour-supportive function of macrophages, e.g. via upregulation of lipid metabolism (43). Moreover, both AP1 and AFT3 are known to be active in hypoxic conditions and may well play a significant role in the regulation of functions of hypoxic microglia (29). For the downregulated genes, the chromatin accessibility at the *P2ry12* Mg-GAM marker gene promoter ATACseq peak was almost completely lost in BV2 cells after co-culture with glioma cells in hypoxic conditions (**Figure 6F** and **Supplemementary Table S6**). The TFs with binding motifs in this peak included SPI1 (also known as PU.1) and IRF8, both known to play essential roles in the regulation of microglial cell identity and function, as well as regulation of *P2ry12* expression (**Figure 6F** and **Supplementary Table S6**) (44–46). In addition, we found that expression of *Spi1* decreased in hypoxic conditions in our RNAseq analysis, which additionally may contribute to the downregulation of *P2ry12* expression in hypoxia (**Figure 6F**). Motifs of other TFs involved in myeloid cell functions were also identified in this peak, including STAT1 and ETS1/2, although these have not been previously directly linked to the regulation of *P2ry12* expression (47). Regulation of expression of *Olfml3* in BV2 cells in our model also had an interesting pattern, as it clearly followed the changes in the chromatin accessibility at its 3'UTR region (**Figure 6G**). Co-culture with glioma cells upregulated the expression of *Olfml3* in BV2 cells, which was then inhibited in hypoxic

conditions. From the TF motifs found in the hypoxia-regulated chromatin accessibility peak in the *Olflm3* gene, the IRF3, SP1, and ETS2 TFs were previously linked with the regulation of immune responses in myeloid cells (**Figure 6G** and **Supplementary Table S6**) (39,48,49). Overall, our data indicate that although chromatin accessibility changes only partially correspond with the strong gene expression changes in hypoxia, some of these concordant alterations may well play a role in defining the myeloid cell properties.

Finally, we tested if the myeloid markers genes that were concordantly regulated at the chromatin and mRNA levels in hypoxic co-cultures, correlate with the "hypoxic score" in GBM GAMs *in vivo*. The correlation analysis in mouse and human GBM datasets between the "hypoxic score" and expression of particular genes indicated *P2ry12* and *Olfml3* as negatively correlated and *Gpnmb*, *Lgals3*, *Tnfaip3*, *Cxcl10*, as well as hypoxic GAM markers as positively correlated either in all GAMs or at least in Mg GAMs (**Figure 5H-J** and **Supplementary Table S7**). Interestingly, some of the genes were inversely correlated with "hypoxic score" than determined in the co-culture model, including *MndaI*, *Cd37* or *S100a11.* We cannot exclude that other factors could contribute to their expression in hypoxic cells *in vivo*.

DISCUSSION

The role of hypoxic stress as a factor affecting myeloid cell identity has not been addressed up to date. Using a well-defined and controllable *in vitro* model of glioma-microglia co-cultures, we show that hypoxia is a strong, differentiating factor, which significantly reprograms chromatin accessibility and gene expression in microglial cells co-cultured with glioma cells. The analysis of concordant changes in chromatin accessibility and gene expression indicates upregulation of genes associated with tumour-supportive functions of microglia (migration, invasion, immunosuppression), while genes involved in homeostatic and neuroprotective

functions, along with canonical microglial markers, are downregulated. We provide evidence that most of the phenotypic subpopulations of GAMs may be influenced to some extent by internal hypoxic tumour stress. Deeper and more detailed microglial, monocytic and macrophage cluster analysis in single-cell RNAseq datasets is needed to allow the detection of these distinct changes.

The "hypoxic score" in GAMs often correlates with the expression of functional lipid GAM marker genes, e.g. *Lgals3* or *Gpnmb*, and it is well established that hypoxia regulates lipid metabolism, lipid processing and storage (50). However, some of the lipid marker genes in GAMs, in addition to lipid uptake and metabolism, can play versatile roles in tumours. For example, Galectin-3 *(LGALS3*) expressed in GAMs was shown to stimulate glioma cell migration and invasion, impair the inflammatory phenotype and overall promote the immunosuppressive environment (51). In breast cancer, the hypoxia-induced expression and secretion of Galectin-3 in TAMs was also responsible for supporting the tumour progression (52). Although *Lgals3* expression is already much higher in Mo/Mφ-GAMs which are more abundant in the tumour core than in Mg-GAMs (5,6), the further upregulation of *Lgals3* in hypoxic GAMs and overall in all cells present in hypoxic regions, including glioma cells, may have a cumulative effect in supporting the glioma progression. Further studies are needed to explore the therapeutic potential of targeting Galectin-3, particularly in tumours with high hypoxia levels.

Tumour hypoxia-dependent reprogramming of chromatin can act as a master regulator of some changes that are essential for the myeloid cell identity, as shown for the repression of microglial marker *P2ry12* and the complete loss of its promoter openness in hypoxia. We have found that such profound downregulation of chromatin accessibility at the *P2ry12* promoter occurred only when microglia cells were exposed to hypoxia in the presence of glioma cells and not in hypoxic BV2 monocultures. Thus, additional signals are required to decrease chromatin accessibility at

the *P2ry12* promoter and block access for IRF8 or SPI1 TFs, which are key regulators of microglial cell identity and specification (44–46). Further work is needed to decipher the precise molecular mechanisms of such regulation in tumour hypoxic conditions.

Due to uniform changes observed for the *Lgals3* upregulation and *P2ry12* downregulation in hypoxic conditions across different murine myeloid cell types and in human scRNAseq and IvyGAP datasets, we speculate that hypoxia-enforced regulation of chromatin and gene expression may employ similar mechanisms across the mouse and human species. In addition, similar hypoxia-dependent mechanisms may dominate the transcriptional response in multiple cell types present within the hypoxic niche. However, our data suggests that interactions with glioma cells, either through direct cell-to-cell contacts or through secreted factors, may impose additional chromatin changes, which will likely dictate the tissue-specific expression of particular genes.

While hypoxia imposes extensive global changes in the chromatin accessibility in BV2 cells, only some of these changes are concordant with gene expression changes occurring in the cells. Several scenarios could explain these discrepancies. It is possible that the chromatin accessibility-dependent changes require more time under hypoxia to translate into actual gene expression changes, while the HIF family TFs or other transcription factor-mediated changes are more rapid and direct, allowing a very quick adaptation to hypoxic conditions (53). Moreover, some chromatin accessibility changes in hypoxia might be the result of changes in long-range contacts in the chromatin 3D structure and do not directly influence the expression of nearby genes (54). Therefore future studies are needed to further examine the significance of all chromatin accessibility changes in glioma-co-cultured hypoxic microglial cells.

Altogether, our data shows that hypoxia has a strong impact on the reprogramming of myeloid cell markers defining cell identity or phenotypic state. To a large extent, the changes in gene

expression are likely to be regulated through the immediate action of transcriptional factors activated in hypoxia with the enriched motifs in the promoters of these markers, including HIF-1α/HIF-2α, NF-κB, RUNX1 AP1 etc. However, in some cases, hypoxia-dependent reprogramming of chromatin will also regulate the expression of myeloid marker genes, as we pointed out for *P2ry12* or *Olfml3*-microglial markers or lipid-GAMs related genes such as *Lgals3* or *Gpnmb*. Here, we provide a robust and reproducible model for studying the direct glioma-microglia interactions, which is suitable for the dissection of hypoxia-dependent mechanisms in GAMs in strictly oxygen-regulated and cross-linking-preserved conditions.

MATERIALS AND METHODS

Cell lines

GL261 mouse glioma cells stably expressing pEGFP-N1 were cultured in DMEM with 10% FBS) and were obtained from Prof. Helmut Kettenman (MDC, Berlin, Germany) (5,24). The murine immortalised BV2 microglia cell line (received from Prof. Klaus Reymann from Leibniz Institute for Neurobiology) and the murine macrophage cell line RAW 264.7 (from Biological Resource Center ICLC Cell bank, #ICLC ATL02001) were cultured in DMEM with GlutaMAX™, supplemented with 2% and 10% FBS, respectively. Bone marrow-derived macrophages (BMDMs) were obtained from C57BL/6 mice at the age of 10-16 weeks, according to the protocol by Toda et al., with some modifications (55). In brief, bone marrow cells from the femur and tibia of mice were collected by a short centrifugation of the bones after removing the epiphyses. Erythrocytes were removed with the use of a dedicated lysis buffer (BD Pharm Lyse™ Lysing Buffer # 555899). Bone marrow cells were frozen in 10% DMSO/FBS. For differentiation into BMDMs, bone marrow cells were plated on glass

coverslips in 6-well plates (1,6 mln cells/well) in DMEM w/Glutamax (Gibco 31966047) supplemented with 10% FBS and 50 ng/ml M-CSF. Culture medium was replaced with fresh medium (containing 10% FBS and 50 ng/ml M-CSF) at day 4 and 6. Additionally, M-CSF was added (50 ng/ml) to the medium on other days if the cultures were detaching from the plates. The BMDMs were used for hypoxic treatment on day 10, at which time the expression of macrophage markers was confirmed with qPCR (not shown). Antibiotics (100 U/mL penicillin, 100 µg/mL streptomycin) were supplemented in all cell culture media. All cell lines were maintained in a humidified atmosphere of CO2/air (5%/95%) at 37°C. The regular mycoplasma tests were carried out on all cells used.

Hypoxic condition and treatment

Cells were incubated at <0.1 or 1% O_2 in a M35 Hypoxystation (Don Whitley) hypoxic chamber in the presence of 5% CO_2 at 37°C for 16h. The hypoxia-mimetic agent $CoCl_2$, at a concentration of 250 µM, was applied under standard culture conditions for 16h.

Direct co-culture

GL261 cells were seeded in DMEM supplemented with 10% FBS and antibiotics (100 U/mL penicillin, 100 µg/mL streptomycin). After 24 h, the medium was changed to a microglia culture medium DMEM with GlutaMAX™ supplemented with 2% FBS and antibiotics (100 U/mL penicillin, 100 µg/mL streptomycin) and the BV2 cells were co-seeded onto GL261 cells at a 1:2 ratio relative to GL261 cells. Following 24h, the cells were cultured under normoxic or hypoxic conditions for another 16 hours and used in further assays. The control BV2 group did not contain any glioma cells.

Immunofluorescence

Cells were seeded on glass coverslips in 24-well plates in the same way as described in direct co-culture section. Cells were washed with PBS and 4% PFA was added to fix cells in hypoxic

or normoxic conditions. After 10 min cells were washed with PBS followed by a 10-minute permeabilisation with ice-cold 100% methanol and wash with PBS. After 1 hour blocking (3% donkey serum, 1% BSA, 0.3% Triton X-100, PBS) the H3K9me3 antibody (1:500, Millipore, Cat#07-442) or H3K27me3 antibody (1:500, Millipore, Cat#07-449) diluted in a blocking solution were added and incubated for 1 hour. This was followed by a triple wash in PBST and an hour incubation in the blocking solution with a secondary donkey anti-rabbit antibody conjugated with Alexa Fluor-555 (1:2000, Invitrogen, Cat#A31572,). Coverslips were washed 3x with PBST and stained with DAPI (1:1000) for 10 min. This was followed by a double wash with PBS and with distilled water and mounting on slides using a mounting solution (Dako).

qPCR

RNA was isolated using RNeasy Mini Kit (QIAGEN,), followed by quality and quantity assessment using NanoDrop 2000 Spectrophotometer (ThermoFisher). cDNA was synthesized from total RNA using SuperScript IV Reverse Transcriptase (Invitrogen). qPCR was performed with the SYBR Green PCR Master Mix Kit (Applied Biosystems) in QuantStudio 12K Flex Real-Time PCR thermocycler (Applied Biosystems) with a listed set of primers (**Supplementary Table S8**). The amplified product was normalized to the 18S housekeeping gene. mRNA fold change was calculated using the 2–ΔΔCt method. The qPCR graphs show the mean ± SD of three biological replicates and statistical significance assessed with two-tailed student t-tests for each gene(* $p<0.05$, ** $p<0.01$, *** $p<0.001$, ns = non-significant), performed with Graph Pad Prism software.

Western blotting

Cells were washed in PBS and lysed in SDS lysis buffer (10 mM Tris-Cl, pH 7.5, 0.1 mM EDTA, 0.1 mM EGTA, 0.5% SDS, 0.1 mM β-mercaptoethanol, protease/phosphatase inhibitors), followed by sonication and centrifugation, as described before (56). Lysates with

equal amount of proteins were subjected to SDS-PAGE and western blotting. After blocking, the following primary antibodies were used: LGALS3 (1:1000, Biolegend. Cat#125401), HIF-1α (1:1000, Abcam, Cat#179483), β-actin (Sigma-Aldrich, Cat#A3854). An enhanced chemiluminescence detection system (ECL) and Chemidoc Imaging System (BioRad) were used to develop the signal from HRP-conjugated secondary antibodies.

IvyGAP human glioblastoma data

Expression of hypoxia-inducible genes (*SLC2A1, VEGFA*), monocytic markers (*LGALS3*) or microglia markers (*P2RY12, TMEM119*) has been tested in the transcriptional atlas of human glioblastoma, where samples for the RNAseq analysis had been collected via microdissection from anatomic structures within glioblastoma (Ivy Glioblastoma Atlas Project; http://glioblastoma.alleninstitute.org/) (23). The violin plots showing the expression z-scores were generated with R programming environment (version 4.2.2, https://www.r-project.org/).

RNAseq

Cells from hypoxia or normoxia conditions were fixed on ice with 3% Glyoxal fixation solution as was described previously (25). For staining of microglia cells CD45 (Clone 30-F11) labeled with PE, (1:400, BD Pharmingen, Cat# 553081) was used. CD45+ cells or GFP+ cells were sorted to 1% BSA in PBS using Cell Sorter BD FACSAriaII. RNA was isolated using RNeasy Plus Kit (Qiagen) according to manufacturer's instructions and the quality was assessed with the Agilent 2100 Bioanalyzer with an RNA 6000 Pico Kit (Agilent Technologies). PolyA-enriched RNA libraries were prepared with the KAPA Stranded mRNA Sample Preparation Kit (Kapa Biosystems). The RNAseq libraries were sequenced at 2x151 bp paired-end on NovaSeq 6000 at the Laboratory of Sequencing (Nencki Institute). Two biological replicates per condition were analysed.

RNAseq data processing and analysis

The quality of raw fastq data was assessed using FASTQC software (https://www.bioinformatics.babraham.ac.uk/projects/fastqc/). Low-quality reads and adapters were trimmed using Trimmomatic (version 0.36) (57). The resulting RNA sequencing reads were mapped to mm10 reference genome sequence using STAR aligner (version 2.6) (58). Read duplicates were marked with Picard Tools (version 2.17.1, https://broadinstitute.github.io/picard/) and only uniquely maped reads were kept for the downstream analysis with samtools view -q 255. Quantification of mapped reads and summarisation by gene was performed using HTSeq-count [PMC4287950] (version 0.9.1), with reverse stranded mode (-s reverse). Differential analysis was performed using Bioconductor package DESeq2 (59). Genes that had significant (Benjamini and Hochberg-corrected P-value <0.05 and |log2 fold change| >=1) changes in their expression levels were called as differentially expressed. Gene ontology (GO) enrichment analysis was done using enrichGO form clusterProfiler (60). Revigo and Cytoscape (version 3.10.2, https://cytoscape.org/) were used to summarise and visualise the GO-enriched terms (61). Motif enrichment analysis for selected genes was performed using HOMER findMotifs.pl (http://homer.ucsd.edu/homer/motif/) for known TF motifs with the default parameters. All sequencing track were generated by Integrative Genome Viewer (IGV) using a normalized bigWig file created with bamCoverage of DeepTools and normalized to genome coverage - RPGC (62,63). The averaged signal across all regions for the two replicates in each condition was calculated using bigwigCompare of DeepTools (62,63) to generate a combined BigWig file. The RNAseq data generated in this project will be deposited at the NCBI platform upon manuscript publication after peer review.

ATACseq

ATACseq was performed as previously described with some modifications (31). While still in hypoxic conditions, cells were fixed with 1% formaldehyde (Thermo Scientific) for 10 min and

then quenched with 0.125 M glycine for 5 min at room temperature. After returning to normal conditions (21% O_2), cells were washed with PBS and incubate in 3% BSA (Sigma) with CD16/CD32 Fc Block™ (1:250, BD Pharmingen, Cat#553142) for 15 min. Next the CD45 (Clone 30-F11) labeled with PE, (1:400, BD Pharmingen, Cat#553081) was added for 40 min, washed with PBS, and CD45+ cells or GFP+ cells were sorted to 1% BSA in PBS using Cell Sorter BD FACSAriaII. After sort, cells were counted and 50,000 cells lysed in cold lysis buffer (10 mM Tris-HCl, pH 7.4, 10 mM NaCl, 3 mM MgCl2 and 0.1% IGEPAL CA-630) for 5 min on ice. Cells were then centrifuged at 500xg for 8min, and cell pellets were resuspended in transposition reaction according to the standard ATACseq protocol using 2.5 ul of Tn5 enzyme per 50 000 of cells (64). After transposition, cells were centrifuged and reverse crosslinked (50 mM Tris-Cl, 1 mM EDTA, 1% SDS, 0.2 M NaCl, 200 µg/ml proteinase K) at 65°C with an overnight shaking at 1200 rpm. Zymo DNA Clean & Concentrator-5 columns (ZymoResearch) were used to purify DNA and the sequencing libraries were prepared according to the original ATACseq protocol (64). The ATACseq libraries were assessed for appropriate quality using a Bioanalyzer 2100 and subjected to paired-end sequencing (2x151bp) using NovaSeq 6000 (Illumina) at the Laboratory of Sequencing (Nencki Institute). n = 2 replicates per condition were analyzed.

ATACseq data processing and analysis

The quality of raw fastq data was assessed using FASTQC software (https://www.bioinformatics.babraham.ac.uk/projects/fastqc/). Reads were trimmed using Trimmomatic (version 0.36) to remove adapter, transposase sequence short reads, and low quality 5′ and 3′ bases (57). Paired-end reads were then aligned to mm10 reference genome using Hisat2 (version 2.1.0) with parameters -X 2000 (65). Duplicate reads were subsequently removed with Picard's MarkDuplicates tool (version 2.26.2, https://broadinstitute.github.io/picard/), and reads mapping to the mitochondrial genome were

also excluded. Only properly paired and uniquely mapped reads were kept for downstream analysis using samtools view with the options -q 30 -f 2 -F 256. Peaks were called using MACS2 (version 2.1.1.2) with parameters set to -f BAPME -q 0.01 –nomodel –shift 0 (66). The obtained peaks were then filtered for peaks overlapping mm10 ENCODE blacklisted genomic regions. To visualize the overlap of open genomic regions (peaks) from different conditions, the makeVennDiagram function from the ChIPpeakAnno package was used with minoverlap parameter set to 200 (67). All sequencing track were generated by IGV using a normalized bigWig file created with deepTools (bamCoverage) and normalized to genome coverage – RPGC (62,63). The ATACseq data generated in this project will be deposited at the NCBI platform upon manuscript publication after peer review. Changes in chromatin accessibility were assessed using edgeR with model that includes all groups (59). The following steps were performed to create a set of consensus ATAC peaks for the read count matrix. First, peaks for two replicates in each condition were intersected and only peaks with overlap > 200 bp were included. Then obtained peaks from all conditions were merged with reduction of overlapping regions using the "reduce" function from the GenomicRanges package to generate consensus peak lists (68). Peaks with FDR < 0.05 (Benjamini and Hochberg - corrected P-value) and |log2 fold change| >= 0.6 were classified as significantly different.

Annotation for differential ATACseq peaks to genomic features

The peaks were annotated to genomic features using ChIPseeker, with the promoter region defined as +/- 2,000 bp around the transcription start site (TSS) and the overlap parameter set to 'all' to annotate peaks to the nearest gene (69). Each peak was annotated to only one genomic feature according to the default annotation priority in ChIPseeker. To assign promoter peaks to all possible genes, a custom-written script in R was used based on biomaRt (68,70) and GenomicRanges packages (70). Functional enrichment analysis of differentially accessible regions nearby genes was performed using enrichGO function from clusterProfiler (60). Revigo

tool was used to merge similar GO terms and visualisation (61). Motif enrichment analysis for selected ATAC-seq peaks was performed using HOMER findMotifsGenome.pl (http://homer.ucsd.edu/homer/motif/) for known TF motifs with the option -size given. For local motif analysis in ATAC-seq peaks, FIMO from the MEME suite was used (71). For the figures, enriched motifs were shown after further filtering to include only those motifs with q-value < 0.01 and where the expression of the transcription factor gene was sufficiently high, defined as a sum of the log2-transformed CPM values across the samples of at least 2.

Analysis of human and mouse scRNAseq data

UMAP plots were created using single-cell RNA sequencing data from mouse tumour-associated macrophages and two human tumour-associated macrophage datasets from Antunes et al., (GSE163120) (6). The data were analyzed in RStudio (R version 4.2.2 (2022-10-31); Platform: x86_64-pc-linux-gnu (64-bit); Running under: Ubuntu 22.04.1 LTS); BiocManager_1.30.19) and Seurat (v 5.0.1). UMAP dimensions and cell labelling were applied as in the original publication (6). Visualizations were generated using built-in Seurat functions, ggplot2 (v 3.5.1), Nebulosa (v 1.8.0)(72), scCustomize (v 1.1.3) (https://doi.org/10.5281/zenodo.5706431), and RColorBrewer (v 1.1-3). Module "hypoxia score" was computed using the Addmodulescore() function from the Seurat library with selected marker genes for the chosen processes. Correlations between selected marker genes and "hypoxia score" were calculated using the Spearman correlation coefficient with the cor() function. The values were visualized on heatmaps (pheatmap_1.0.12).

ACKNOWLEDGMENTS

We thank Pawel Segit and Karol Jacek for their support in the bioinformatic analyses. We thank Bartek Gielniewski from the Sequencing Core Facility at the Nencki Institute for sequencing the samples.

FUNDING

Studies were supported by the National Science Center grant (Poland) 2019/33/B/NZ1/01556.

FIGURE LEGENDS

Figure 1. Hypoxia dysregulates the expression of *Lgals3, P2ry12* and *Tmem119* in myeloid cells and in GBM samples in vivo.

A, Expression analysis using qPCR of *Lgals3* in BV2, RAW 264.6 and BMBM cells, as indicated in relation to 18S housekeeping gene. *Glut1* (*Slc2a1*) and *Vegfa* were used as hypoxia controls. The mean fold change with standard deviation (SD) is shown from at least three independent biological replicates. Two-tailed student t-tests test determined the statistical significance (* $p<0.05$, ** $p<0.01$, *** $p<0.001$, ns = non-significant).

B, BV2 and RAW 264.7 cell line was exposed to 21% or <0.1% O_2 for 16 h and subjected to western blotting for the LGALS3. HIF-1α was used as a hypoxia control. A representative experiment of three independent repeats is shown.

C, Expression analysis using qPCR of *P2ry12 and Tmem119* in BV2, RAW 264.6 and BMBM cells, as indicated in relation to 18S housekeeping gene. The mean fold change with standard deviation (SD) is shown from at least three independent biological replicates.

D, UMAP plot showing clusters of monocytes and TAMs subpopulation from mouse GL261 tumours as identified in the public scRNA-seq dataset (GSE163120) (6).

E, UMAP plot showing the expression of hypoxia score in the dataset from (**D**).

F-H, UMAP plots showing the expression of (**F**) *Lgals3*, (**G**) *Tmem119* and (**H**) *P2ry12* in the dataset from (**D**).

I, Heatmaps representing the correlation matrix between hypoxia score and *P2ry12*, *Tmem119* and *Lgals3* expression in mouse GL261 tumors, human newly diagnosed GBM and human recurrent GBM scRNA-seq datasets (all data from GSE163120).

J, Violin plots showing z-score expression of hypoxia-inducible genes *VEGFA* and *SLC2A1*, as well of *TMEM119*, *P2RY12 and LGALS3 genes* in different anatomical regions of GBM samples, from Ivy GBM Atlas Project (Ivy GAP; https://glioblastoma.alleninstitute.org/) (23). LE, leading edge; IT, infiltrating tumour; CT, cellular tumor; CTpnz, perinecrotic zone; CTpcan, pseudopalisading cells around necrosis; CThbv, hyperplastic blood vessels in cellular tumour; CTmvp, microvascular proliferation.

Figure 2. Glioma and hypoxia exposure reprograms the transcriptome of BV2 microglial cells

A, A scheme summarising direct glioma-microglia co-culture experiment.

B, Immunofluorescent images of BV2 and GL261(stably expressing GFP) cells co-cultured in normoxic or hypoxic conditions, as used in the assay in (**A**). Red color visualises actin cytoskeleton stained with phalloidin and blue color marks nuclei stained with DAPI. Green to yellow cells represent GL261 while red-only positive cells are microglia which are negative for GFP.

C, A principal component plot of normalised gene expression for BV2 cells in normoxia (Ctrl_N), in hypoxia (Ctrl_H) or in normoxic co-cultures with glioma (CC_N) and in hypoxic co-cultures with glioma (CC_H).

D-E, Venn diagrams summarising the overlap between differentially (**D**) upregulated and (**E**) downregulated genes in BV2 cells after exposure to hypoxia in the presence (CC) or absence (Ctrl) of glioma cells.

F-G, Dot plot of enriched GO pathways for gene sets significantly (**F**) upregulated or (**G**) downregulated after exposure to hypoxia in coculture with glioma CC. The top 15 GO pathways were selected based on the lowest adjusted p-values, and closely related terms were merged using REVIGO.

H, The heatmap showing a z-score expression for genes up- or downregulated in CC or Ctrl Hypoxic cells.

I, A volcano plot showing significantly up- (2606) or downregulated (1942) genes in glioma co-cultured (CC) microglial cells in purple. Genes with expression additionally increased or decreased in CC versus Ctrl hypoxic conditions are projected in black. Left and right box panels shows examples of genes additionally decreased or increased in CC versus Ctrl, respectively.

Figure 3. Hypoxia dysregulates the expression of multiple monocytic and microglial TAM subcluster marker genes

A, Gene expression changes in RNAseq data from Figure 2 in BV2 cells in response to co-culture with glioma GL261 cells in normoxia (CC), in response to co-culture with glioma GL261 cells in hypoxia (CC+Hyp) and in response to hypoxia only (Hyp) are shown for the genes included in hypoxia score for TAMs. The size of the circle indicates the fold change in a particular comparison. Dark blue and red colors indicate statistically significant gene expression changes (with p adjusted value < 0.05), while pale blue and red colours indicate non-significant regulation (with p adjusted value > 0.05).

B, Gene expression changes in BV2 cells in comparisons as in (**A**) for top Mg-TAM and Mo-TAM marker genes.

C, Gene expression changes in BV2 cells in comparisons as in (**A**) for myeloid marker genes representing specific subpopulations of Mo-TAMs, including lipid, interferon (IFN), chemotactic (Chem), phagocytic (Phago), ribosomal (Ribo) or transitory monocytes.

D, Transcription factor (TF) motif enrichment analysis on the promoters of significantly up- or down-regulated genes from (**A-C**) in BV2 cells after hypoxic co-culture with glioma cells.

Figure 4. Hypoxia-dependent gene expression analysis in GL261 cell monocultures and co-cultures with microglia

A, A scheme indicating the analysis of GL261 transcriptome in co-culture with microglial cells or in monocultures.

B, A principal component plot of normalised gene expression for GL261 cells in normoxia (Ctrl_N), in hypoxia (Ctrl_H) or in normoxic co-cultures with microglia (CC_N) and in hypoxic co-cultures with microglia (CC_H).

C-E, Volcano plots showing differential gene expression in GL261 cells co-cultured with BV2 (**C**) in normoxia, (**D**) in hypoxia or (**E**) as hypoxic monocultures.

F-G, ORA analysis of GO processes enriched in GL261 at the differentially up-regulated genes in hypoxic glioma co-cultures with microglia or in hypoxic monocultures.

Figure 5. Glioma and hypoxia exposure reprograms the epigenome of BV2 cells

A, PCA analysis on identified ATACseq peaks in BV2 cells treated with hypoxia (<0.1% O2) or normoxia in the presence or absence of glioma cells.

B, Bar plots showing differentially regulated ATACseq peak counts annotated to specific genomic regions, as indicated in the figure legend. Three differential analyses were performed for chromatin accessibility in BV2 cells: in response to co-culture with glioma GL261 cells in normoxia (CC), BV2 in response to co-culture with glioma GL261 cells in hypoxia (CC+Hyp) and in response to hypoxia only (Hyp).

C-D, Venn diagrams summarising common and distinct upregulated (**C**) or downregulated (**D**) ATACseq peaks at promoters in BV2 cells treated with CC, CC+Hyp or Hyp.

E-F, Analysis of HIF metagene score in ATACseq pekas at the **(E)** gene promoter and **(F)** promoters and gene bodies (denoted as genic) in BV2 cell in hypoxia. HIF metagene set was defined by Lombardi et al (26). The average ATACseq signal of the HIF metagene score is represented as read counts per million. Two-way ANOVA determined the statistical significance.

G, Enrichment of TF motifs in ATACseq peaks at the gene promoter or genic regions that increased in BV2 cells treated with hypoxia in coculture with GL261 (CC) or alone (Ctrl) in comparison to respective CC or Ctrl normoxic cells. Circle size indicates the percentage of sequences in the subset with the motif, while the colour gradient reflects the significance of enrichment. All indicated enriched TF motifs are statistically significant (p adjusted<0.05).

H-I, Overrepresentation analysis showing GO processes in downregulated (**H**) or upregulated (**I**) genic ATACseq peaks. The top 15 GO processes were selected based on the lowest adjusted p-values, and closely related terms were merged using REVIGO. The gradient of colours indicates the gene count in each associated process.

Figure 6. Concordant hypoxia-dependent transcriptomic and epigenomic changes in glioma-co-cultured BV2 cells impact myeloid cell functional markers

A, A dot plot showing the correlation of RNA expression changes versus maximal ATACseq peak fold changes per gene. Statistically significant pearson (p.cor) and spearman (s.cor) correlation coefficient values are shown.

B-C, Venn diagrams showing concordantly upregulated (**B**) or downregulated (**C**) gene expression and corresponding genic ATACseq peaks in BV2 cells treated with hypoxic co-culture with glioma cells. The rectangular frames indicate myeloid marker genes from Figure 3 identified in the concordant ATACseq and RNAseq changes.

D-G, The mRNA expression (RNAseq) and ATACseq profiles (from Integrative Genomics Viewer, IGV) for concordantly upregulated (*Gpnmb* (**D**) and *Lgals3* (**E**)) and downregulated (*P2ry12* (**F**) and *Olfml3* (**G**)) genes in BV2 cells treated with hypoxia co-culture with GL261 cells. The FIMO analysis was used for the selected ATACseq peaks, to identify available motifs for TFs, as indicated in rectangular boxes under each gene. The IGV track shown are the average from two biological repeats.

H-J, Heatmaps representing the correlation matrix between hypoxia score and concordantly hypoxia-regulated genes at the expression and chromatin level indicated in (**B**) and (**C**) in scRNAseq datasets for mouse TAMs (**H**), TAMs in human newly diagnosed GBM (**I**) and TAMs in human recurrent GBM (**J**) (all from GSE163120) (6).

REFERENCES

1. Louis DN, Perry A, Wesseling P, Brat DJ, Cree IA, Figarella-Branger D, et al. The 2021 WHO classification of tumors of the central nervous system: A summary. Neuro Oncol. 2021;23(8).

2. Neftel C, Laffy J, Filbin MG, Hara T, Shore ME, Rahme GJ, et al. An Integrative

Model of Cellular States, Plasticity, and Genetics for Glioblastoma. Cell. 2019;178(4).

3. Khan F, Pang L, Dunterman M, Lesniak MS, Heimberger AB, Chen P. Macrophages and microglia in glioblastoma: heterogeneity, plasticity, and therapy. Vol. 133, Journal of Clinical Investigation. 2023.

4. Quail DF, Joyce JA. The Microenvironmental Landscape of Brain Tumors. Vol. 31, Cancer Cell. 2017.

5. Ochocka N, Segit P, Walentynowicz KA, Wojnicki K, Cyranowski S, Swatler J, et al. Single-cell RNA sequencing reveals functional heterogeneity of glioma-associated brain macrophages. Nat Commun. 2021;12(1).

6. Pombo Antunes AR, Scheyltjens I, Lodi F, Messiaen J, Antoranz A, Duerinck J, et al. Single-cell profiling of myeloid cells in glioblastoma across species and disease stage reveals macrophage competition and specialization. Nat Neurosci. 2021;24(4).

7. Sankowski R, Süß P, Benkendorff A, Böttcher C, Fernandez-Zapata C, Chhatbar C, et al. Multiomic spatial landscape of innate immune cells at human central nervous system borders. Nat Med. 2024;30(1).

8. Wang W, Li T, Cheng Y, Li F, Qi S, Mao M, et al. Identification of hypoxic macrophages in glioblastoma with therapeutic potential for vasculature normalization. Cancer Cell [Internet]. 2024;42(5):815-832.e12. Available from: https://doi.org/10.1016/j.ccell.2024.03.013

9. Yabo YA, Moreno-Sanchez PM, Pires-Afonso Y, Kaoma T, Nosirov B, Scafidi A, et al. Glioblastoma-instructed microglia transition to heterogeneous phenotypic states with phagocytic and dendritic cell-like features in patient tumors and patient-derived orthotopic xenografts. Genome Med [Internet]. 2024;16(1):1–29. Available from:

https://doi.org/10.1186/s13073-024-01321-8

10. Ravi VM, Will P, Kueckelhaus J, Sun N, Joseph K, Salié H, et al. Spatially resolved multi-omics deciphers bidirectional tumor-host interdependence in glioblastoma. Cancer Cell. 2022;40(6):639-655.e13.

11. Kloosterman DJ, Erbani J, Boon M, Farber M, Handgraaf SM, Ando-Kuri M, et al. Macrophage-mediated myelin recycling fuels brain cancer malignancy. Cell [Internet]. 2024;1–21. Available from: http://www.ncbi.nlm.nih.gov/pubmed/39137777

12. Ochocka N, Segit P, Wojnicki K, Cyranowski S, Swatler J, Jacek K, et al. Specialized functions and sexual dimorphism explain the functional diversity of the myeloid populations during glioma progression. Cell Rep. 2023;42(1).

13. Hara T, Chanoch-Myers R, Mathewson ND, Myskiw C, Atta L, Bussema L, et al. Interactions between cancer cells and immune cells drive transitions to mesenchymal-like states in glioblastoma. Cancer Cell. 2021;39(6).

14. Sattiraju A, Kang S, Giotti B, Chen Z, Marallano VJ, Brusco C, et al. Hypoxic niches attract and sequester tumor-associated macrophages and cytotoxic T cells and reprogram them for immunosuppression. Immunity [Internet]. 2023;56(8):1825-1843.e6. Available from: https://doi.org/10.1016/j.immuni.2023.06.017

15. Greenwald AC, Darnell NG, Hoefflin R, Simkin D, Mount CW, Gonzalez Castro LN, et al. Integrative spatial analysis reveals a multi-layered organization of glioblastoma. Cell. 2024;187(10):2485-2501.e26.

16. Hammond EM, Asselin MC, Forster D, O'Connor JPB, Senra JM, Williams KJ. The Meaning, Measurement and Modification of Hypoxia in the Laboratory and the Clinic. Clin Oncol. 2014;26(5).

17. Liao C, Zhang Q. Understanding the Oxygen-Sensing Pathway and Its Therapeutic Implications in Diseases. Vol. 190, American Journal of Pathology. 2020.

18. Sadozai H, Acharjee A, Kayani HZ, Gruber T, Gorczynski RM, Burke B. High hypoxia status in pancreatic cancer is associated with multiple hallmarks of an immunosuppressive tumor microenvironment. Front Immunol. 2024;15.

19. Gu X, Meng H, Wang J, Wang R, Cao M, Liu S, et al. Hypoxia contributes to galectin-3 expression in renal carcinoma cells. Eur J Pharmacol. 2021;890.

20. Bou-Gharios J, Noël G, Burckel H. Preclinical and clinical advances to overcome hypoxia in glioblastoma multiforme. Cell Death Dis [Internet]. 2024;15(7):1–12. Available from: http://dx.doi.org/10.1038/s41419-024-06904-2

21. Leszczynska KB, Foskolou IP, Abraham AG, Anbalagan S, Tellier C, Haider S, et al. Hypoxia-induced p53 modulates both apoptosis and radiosensitivity via AKT. J Clin Invest. 2015;125(6).

22. Epstein ACR, Gleadle JM, McNeill LA, Hewitson KS, O'Rourke J, Mole DR, et al. C. elegans EGL-9 and mammalian homologs define a family of dioxygenases that regulate HIF by prolyl hydroxylation. Cell. 2001;107(1).

23. Puchalski RB, Shah N, Miller J, Dalley R, Nomura SR, Yoon JG, et al. An anatomic transcriptional atlas of human glioblastoma. Science (80-). 2018;360(6389).

24. Sliwa M, Markovic D, Gabrusiewicz K, Synowitz M, Glass R, Zawadzka M, et al. The invasion promoting effect of microglia on glioblastoma cells is inhibited by cyclosporin A. Brain. 2007;130(2).

25. Channathodiyi P, Houseley J. Glyoxal fixation facilitates transcriptome analysis after antigen staining and cell sorting by flow cytometry. PLoS One. 2021;16(1 January).

26. Lombardi O, Li R, Halim S, Choudhry H, Ratcliffe PJ, Mole DR. Pan-cancer analysis of tissue and single-cell HIF-pathway activation using a conserved gene signature. Cell Rep. 2022;41(7).

27. Liu L, Simon MC. Regulation of transcription and translation by hypoxia. Vol. 3, Cancer Biology and Therapy. 2004.

28. Li ZY, Zhu YX, Chen JR, Chang X, Xie ZZ. The role of KLF transcription factor in the regulation of cancer progression. Vol. 162, Biomedicine and Pharmacotherapy. 2023.

29. Rzymski T, Milani M, Pike L, Buffa F, Mellor HR, Winchester L, et al. Regulation of autophagy by ATF4 in response to severe hypoxia. Oncogene. 2010;29(31).

30. Ameri K, Hammond EM, Culmsee C, Raida M, Katschinski DM, Wenger RH, et al. Induction of activating transcription factor 3 by anoxia is independent of p53 and the hypoxic HIF signalling pathway. Oncogene. 2007;26(2).

31. Leszczynska KB, Dzwigonska M, Estephan H, Moehlenbrink J, Bowler E, Giaccia AJ, et al. Hypoxia-mediated regulation of DDX5 through decreased chromatin accessibility and post-translational targeting restricts R-loop accumulation. Mol Oncol [Internet]. 2023;n/a(n/a). Available from: https://febs.onlinelibrary.wiley.com/doi/abs/10.1002/1878-0261.13431

32. Pires IM, Bencokova Z, Milani M, Folkes LK, Li JA, Stratford MR, et al. Effects of acute versus chronic hypoxia on DNA damage responses and genomic instability. Cancer Res. 2010;70(3).

33. Brady LK, Wang H, Radens CM, Bi Y, Radovich M, Maity A, et al. Transcriptome analysis of hypoxic cancer cells uncovers intron retention in EIF2B5 as a mechanism to

inhibit translation. PLoS Biol. 2017;15(10).

34. Chen X, Shen Y, Draper W, Buenrostro JD, Litzenburger U, Cho SW, et al. ATAC-see reveals the accessible genome by transposase-mediated imaging and sequencing. Nat Methods. 2016;13(12).

35. Vollmann H, Wölfel S, Ohneseit P, Stransky E, Vonthein R, Wick W, et al. Differential expression of Egr1 and activation of microglia following irradiation in the rat brain. Strahlentherapie und Onkol. 2007;183(5).

36. Kim GD, Das R, Goduni L, McClellan S, Hazlett LD, Mahabeleshwar GH. Kruppel-like factor 6 promotes macrophage-mediated inflammation by suppressing B cell leukemia/lymphoma 6 expression. J Biol Chem. 2016;291(40).

37. El-Deeb NK, El-Tanbouly DM, Khattab MA, EL-Yamany MF, Mohamed AF. Crosstalk between PI3K/AKT/KLF4 signaling and microglia M1/M2 polarization as a novel mechanistic approach towards flibanserin repositioning in parkinson's disease. Int Immunopharmacol. 2022;112.

38. Zucker SN, Fink EE, Bagati A, Mannava S, Bianchi-Smiraglia A, Bogner PN, et al. Nrf2 amplifies oxidative stress via induction of Klf9. Mol Cell. 2014;53(6).

39. Guo H, Du M, Yang Y, Lin X, Wang Y, Li H, et al. Sp1 Regulates the M1 Polarization of Microglia Through the HuR/NF-κB Axis after Spinal Cord Injury. Neuroscience. 2024;544.

40. Abutbul S, Shapiro J, Szaingurten-Solodkin I, Levy N, Carmy Y, Baron R, et al. TGF-β signaling through SMAD2/3 induces the quiescent microglial phenotype within the CNS environment. Glia. 2012;60(7).

41. Yalcin F, Haneke H, Efe IE, Kuhrt LD, Motta E, Nickl B, et al. Tumor associated

microglia/macrophages utilize GPNMB to promote tumor growth and alter immune cell infiltration in glioma. Acta Neuropathol Commun [Internet]. 2024;12(1):1–21. Available from: https://doi.org/10.1186/s40478-024-01754-7

42. Zhang F, Wang H, Wang X, Jiang G, Liu H, Zhang G, et al. TGF-β induces M2-like macrophage polarization via SNAILmediated suppression of a pro-inflammatory phenotype. Oncotarget. 2016;7(32).

43. Ku HC, Cheng CF. Master Regulator Activating Transcription Factor 3 (ATF3) in Metabolic Homeostasis and Cancer. Vol. 11, Frontiers in Endocrinology. 2020.

44. Sonn I, Honda-Ozaki F, Yoshimatsu S, Morimoto S, Watanabe H, Okano H. Single transcription factor efficiently leads human induced pluripotent stem cells to functional microglia. Inflamm Regen. 2022;42(1).

45. Butovsky O, Weiner HL. Microglial signatures and their role in health and disease. Vol. 19, Nature Reviews Neuroscience. 2018.

46. Maurya SK, Gupta S, Mishra R. Transcriptional and epigenetic regulation of microglia in maintenance of brain homeostasis and neurodegeneration. Vol. 15, Frontiers in Molecular Neuroscience. 2023.

47. Butturini E, Boriero D, Carcereri de Prati A, Mariotto S. STAT1 drives M1 microglia activation and neuroinflammation under hypoxia. Arch Biochem Biophys. 2019;669.

48. Tarassishin L, Suh HS, Lee SC. Interferon regulatory factor 3 plays an anti-inflammatory role in microglia by activating the PI3K/Akt pathway. J Neuroinflammation. 2011;8.

49. Vázquez-Cabrera G, Škandík M, Roncier N, Real Oualit F, Cruz De Los Santos M, Baleviciute A, et al. ID2-ETS2 axis regulates the transcriptional acquisition of pro-

tumoral microglia phenotype in glioma. Cell Death Dis. 2024;15(7).

50. Munir R, Lisec J, Swinnen J V., Zaidi N. Lipid metabolism in cancer cells under metabolic stress. Vol. 120, British Journal of Cancer. 2019.

51. Rivera-Ramos A, Cruz-Hernández L, Talaverón R, Sánchez-Montero MT, García-Revilla J, Mulero-Acevedo M, et al. Galectin-3 depletion tames pro-tumoural microglia and restrains cancer cells growth. Cancer Lett. 2024;591(October 2023).

52. Wang L, Li YS, Yu LG, Zhang XK, Zhao L, Gong FL, et al. Galectin-3 expression and secretion by tumor-associated macrophages in hypoxia promotes breast cancer progression. Biochem Pharmacol. 2020;178.

53. Taylor CT, Scholz CC. The effect of HIF on metabolism and immunity. Vol. 18, Nature Reviews Nephrology. 2022.

54. Wei X, Xiang Y, Peters DT, Marius C, Sun T, Shan R, et al. HiCAR is a robust and sensitive method to analyze open-chromatin-associated genome organization. Mol Cell. 2022;82(6).

55. Toda G, Yamauchi T, Kadowaki T, Ueki K. Preparation and culture of bone marrow-derived macrophages from mice for functional analysis. STAR Protoc. 2021;2(1).

56. Leszczynska KB, Freitas-Huhtamäki A, Jayaprakash C, Dzwigonska M, Vitorino FNL, Horth C, et al. H2A.Z histone variants facilitate HDACi-dependent removal of H3.3K27M mutant protein in pediatric high-grade glioma cells. Cell Rep. 2024;43(2).

57. Bolger AM, Lohse M, Usadel B. Trimmomatic: A flexible trimmer for Illumina sequence data. Bioinformatics. 2014;30(15).

58. Dobin A, Davis CA, Schlesinger F, Drenkow J, Zaleski C, Jha S, et al. STAR: Ultrafast universal RNA-seq aligner. Bioinformatics. 2013;29(1).

59. Love MI, Huber W, Anders S. Moderated estimation of fold change and dispersion for RNA-seq data with DESeq2. Genome Biol. 2014;15(12).

60. Yu G, Wang LG, Han Y, He QY. ClusterProfiler: An R package for comparing biological themes among gene clusters. Omi A J Integr Biol. 2012;16(5).

61. Supek F, Bošnjak M, Škunca N, Šmuc T. Revigo summarizes and visualizes long lists of gene ontology terms. PLoS One. 2011;6(7).

62. Ramírez F, Ryan DP, Grüning B, Bhardwaj V, Kilpert F, Richter AS, et al. deepTools2: a next generation web server for deep-sequencing data analysis. Nucleic Acids Res. 2016;44(W1).

63. Robinson JT, Thorvaldsdóttir H, Winckler W, Guttman M, Lander ES, Getz G, et al. Integrative genomics viewer. Vol. 29, Nature Biotechnology. 2011.

64. Buenrostro JD, Wu B, Chang HY, Greenleaf WJ. ATAC-seq: A method for assaying chromatin accessibility genome-wide. Curr Protoc Mol Biol. 2015;2015.

65. Kim D, Langmead B, Salzberg SL. HISAT: A fast spliced aligner with low memory requirements. Nat Methods. 2015;12(4).

66. Zhang Y, Liu T, Meyer CA, Eeckhoute J, Johnson DS, Bernstein BE, et al. Model-based analysis of ChIP-Seq (MACS). Genome Biol. 2008;9(9).

67. Zhu LJ, Gazin C, Lawson ND, Pagès H, Lin SM, Lapointe DS, et al. ChIPpeakAnno: A Bioconductor package to annotate ChIP-seq and ChIP-chip data. BMC Bioinformatics. 2010;11.

68. Lawrence M, Huber W, Pagès H, Aboyoun P, Carlson M, Gentleman R, et al. Software for Computing and Annotating Genomic Ranges. PLoS Comput Biol. 2013;9(8).

69. Yu G, Wang LG, He QY. ChIP seeker: An R/Bioconductor package for ChIP peak annotation, comparison and visualization. Bioinformatics. 2015;31(14).

70. Durinck S, Spellman PT, Birney E, Huber W. Mapping identifiers for the integration of genomic datasets with the R/ Bioconductor package biomaRt. Nat Protoc. 2009;4(8).

71. Grant CE, Bailey TL, Noble WS. FIMO: Scanning for occurrences of a given motif. Bioinformatics. 2011;27(7).

72. Alquicira-Hernandez J, Powell JE. Nebulosa recovers single-cell gene expression signals by kernel density estimation. Bioinformatics. 2021;37(16).

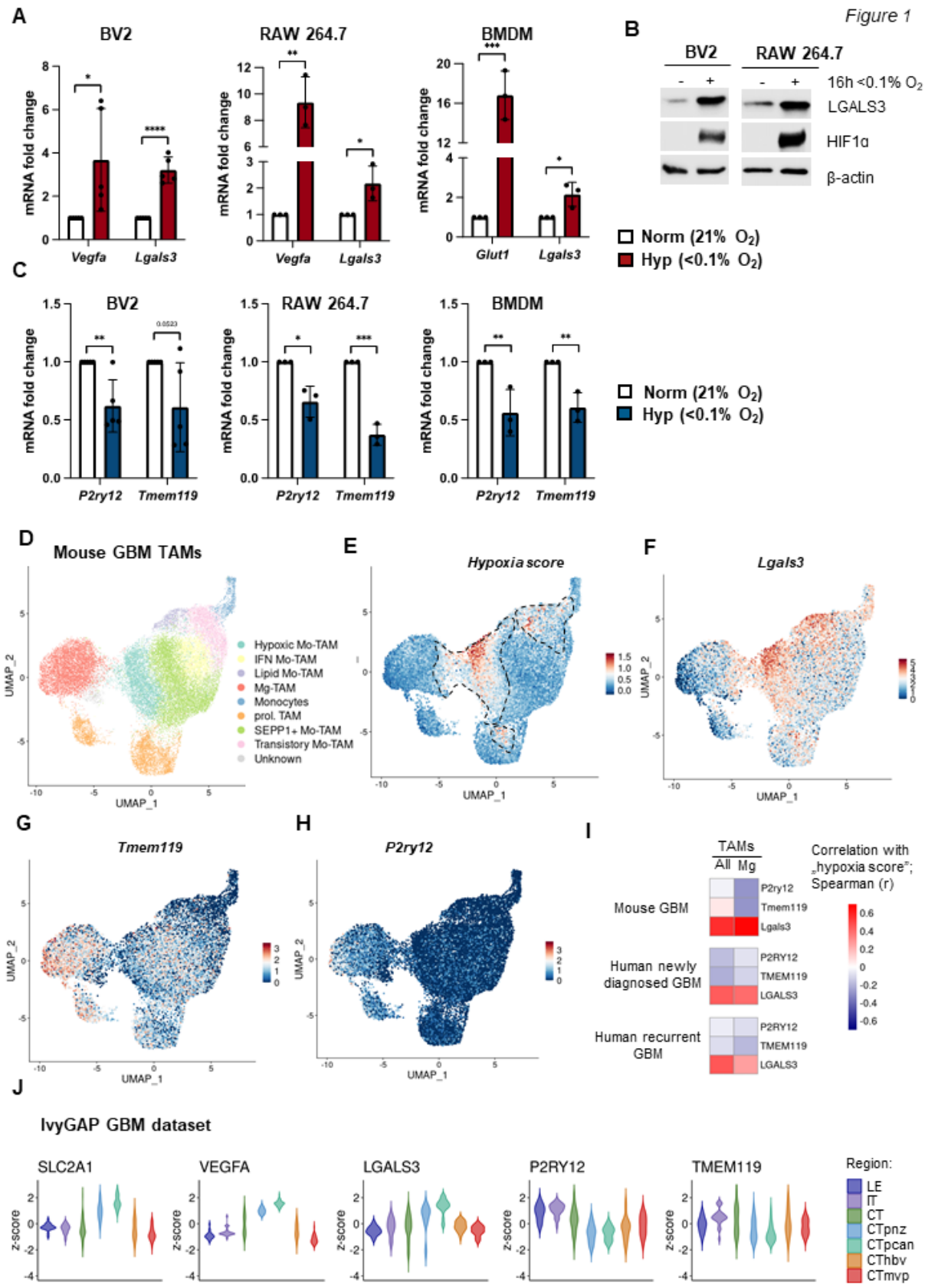
Figure 1
A
BV2
RAW 264.7
BMDM
mRNA fold change
Vegfa
Lgals3
Glut1
B
BV2
RAW 264.7
16h <0.1% O2
LGALS3
HIF1α
β-actin
Norm (21% O2)
Hyp (<0.1% O2)
C
P2ry12
Tmem119
D
Mouse GBM TAMs
Hypoxic Mo-TAM
IFN Mo-TAM
Lipid Mo-TAM
Mg-TAM
Monocytes
prol. TAM
SEPP1+ Mo-TAM
Transistory Mo-TAM
Unknown
UMAP_1
UMAP_2
E
Hypoxia score
F
Lgals3
G
Tmem119
H
P2ry12
I
TAMs
All Mg
Mouse GBM
Human newly diagnosed GBM
Human recurrent GBM
P2ry12
Tmem119
Lgals3
P2RY12
TMEM119
LGALS3
Correlation with „hypoxia score"; Spearman (r)
J
IvyGAP GBM dataset
SLC2A1
VEGFA
LGALS3
P2RY12
TMEM119
z-score
Region:
LE
IT
CT
CTpnz
CTpcan
CThbv
CTmvp

Figure 2

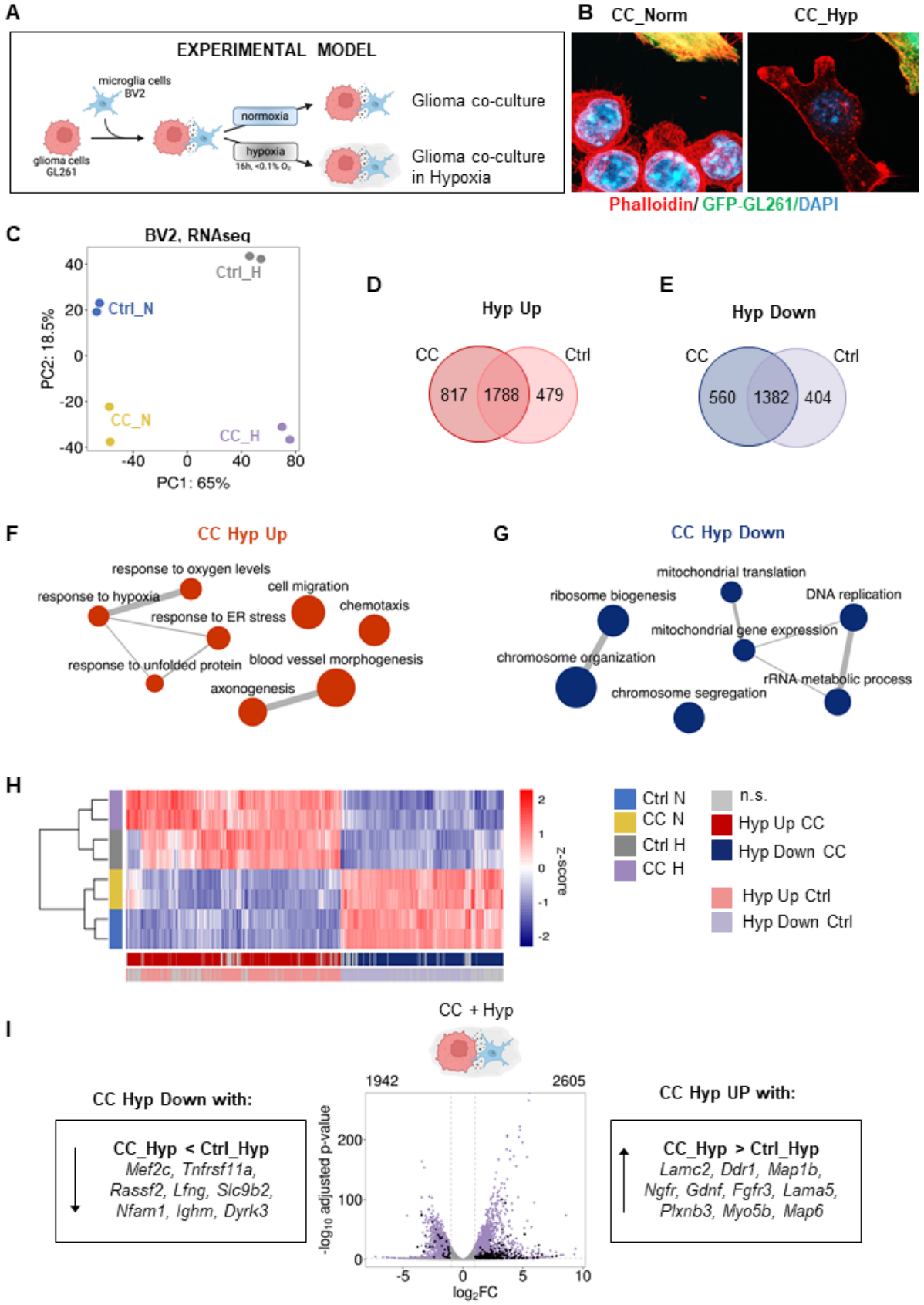
A
EXPERIMENTAL MODEL
microglia cells BV2
glioma cells GL261
normoxia
hypoxia
Glioma co-culture
Glioma co-culture in Hypoxia
B
CC_Norm
CC_Hyp
Phalloidin/ GFP-GL261/DAPI
C
BV2, RNAseq
Ctrl_H
Ctrl_N
CC_N
CC_H
PC2: 18.5%
PC1: 65%
D
Hyp Up
CC
Ctrl
817
1788
479
E
Hyp Down
CC
Ctrl
560
1382
404
F
CC Hyp Up
response to oxygen levels
response to hypoxia
cell migration
chemotaxis
response to ER stress
response to unfolded protein
blood vessel morphogenesis
axonogenesis
G
CC Hyp Down
mitochondrial translation
ribosome biogenesis
DNA replication
mitochondrial gene expression
chromosome organization
rRNA metabolic process
chromosome segregation
H
z-score
Ctrl N
CC N
Ctrl H
CC H
n.s.
Hyp Up CC
Hyp Down CC
Hyp Up Ctrl
Hyp Down Ctrl
I
CC + Hyp
1942
2605
-log10 adjusted p-value
log2FC
CC Hyp Down with:
CC_Hyp < Ctrl_Hyp
Mef2c, Tnfrsf11a, Rassf2, Lfng, Slc9b2, Nfam1, Ighm, Dyrk3
CC Hyp UP with:
CC_Hyp > Ctrl_Hyp
Lamc2, Ddr1, Map1b, Ngfr, Gdnf, Fgfr3, Lama5, Plxnb3, Myo5b, Map6

Figure 3

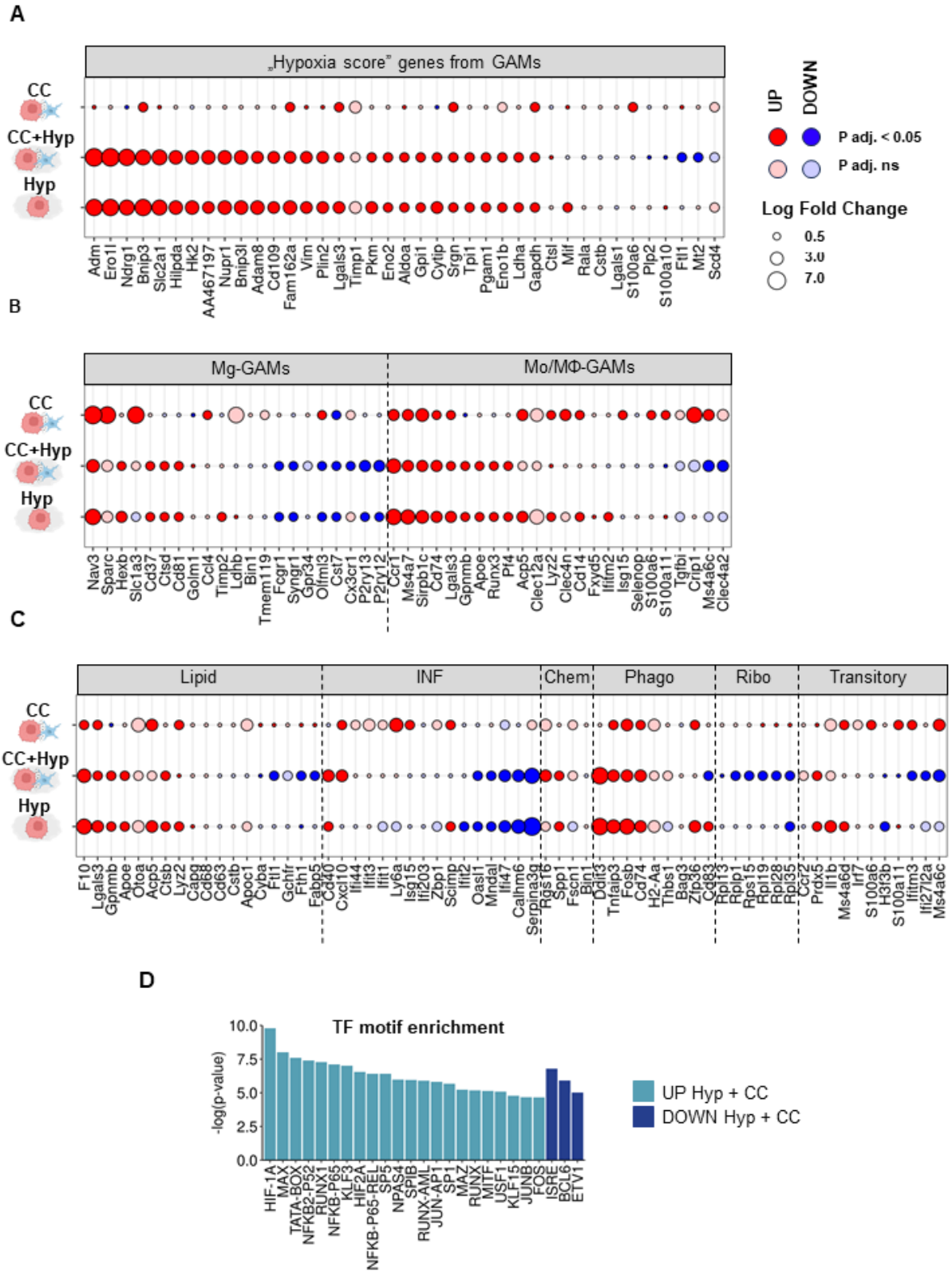
A
„Hypoxia score" genes from GAMs
CC
CC+Hyp
Hyp
Adm
Ero1l
Ndrg1
Bnip3
Slc2a1
Hilpda
Hk2
AA467197
Nupr1
Bnip3l
Adam8
Cd109
Fam162a
Vim
Plin2
Lgals3
Timp1
Pkm
Eno2
Aldoa
Gpi1
Cytip
Srgn
Tpi1
Pgam1
Eno1b
Ldha
Gapdh
Ctsl
Mif
Rala
Cstb
Lgals1
S100a6
Plp2
S100a10
Ftl1
Mt2
Scd4
UP
DOWN
P adj. < 0.05
P adj. ns
Log Fold Change
0.5
3.0
7.0
B
Mg-GAMs
Mo/MΦ-GAMs
Nav3
Sparc
Hexb
Slc1a3
Cd37
Ctsd
Cd81
Golm1
Ccl4
Timp2
Ldhb
Bin1
Tmem119
Fcgr1
Syngr1
Gpr34
Olfml3
Cst7
Cx3cr1
P2ry13
P2ry12
Ccr1
Ms4a7
Sirpb1c
Cd74
Lgals3
Gpnmb
Apoe
Runx3
Pf4
Acp5
Clec12a
Lyz2
Clec4n
Cd14
Fxyd5
Ifitm2
Isg15
Selenop
S100a6
S100a11
Tgfbi
Crip1
Ms4a6c
Clec4a2
C
Lipid
INF
Chem
Phago
Ribo
Transitory
F10
Lgals3
Gpnmb
Apoe
Otoa
Acp5
Ctsb
Lyz2
Capg
Cd68
Cd63
Cstb
Apoc1
Cyba
Ftl1
Gchfr
Fth1
Fabp5
Cd40
Cxcl10
Ifi44
Ifit3
Ifit1
Ly6a
Isg15
Ifi203
Zbp1
Scimp
Ifit2
Oasl1
Mndal
Ifi47
Calhm6
Serpina3g
Rgs16
Spp1
Fscn1
Bin1
Ddit3
Tnfaip3
Fosb
Cd74
H2-Aa
Thbs1
Bag3
Zfp36
Cd83
Rpl13
Rplp1
Rps15
Rpl19
Rpl28
Rpl35
Ccr2
Prdx5
Il1b
Ms4a6d
Irf7
S100a6
H3f3b
S100a11
Ifitm3
Ifi27l2a
Ms4a6c
D
TF motif enrichment
-log(p-value)
10.0
7.5
5.0
2.5
0.0
HIF-1A
MAX
TATA-BOX
NFKB2-P52
RUNX1
NFKB-P65
KLF3
HIF2A
NFKB-P65-REL
SP5
NPAS4
SPIB
RUNX-AML
JUN-AP1
SP1
MAZ
RUNX
MITF
USF1
KLF15
JUNB
FOS
ISRE
BCL6
ETV1
UP Hyp + CC
DOWN Hyp + CC

Figure 4

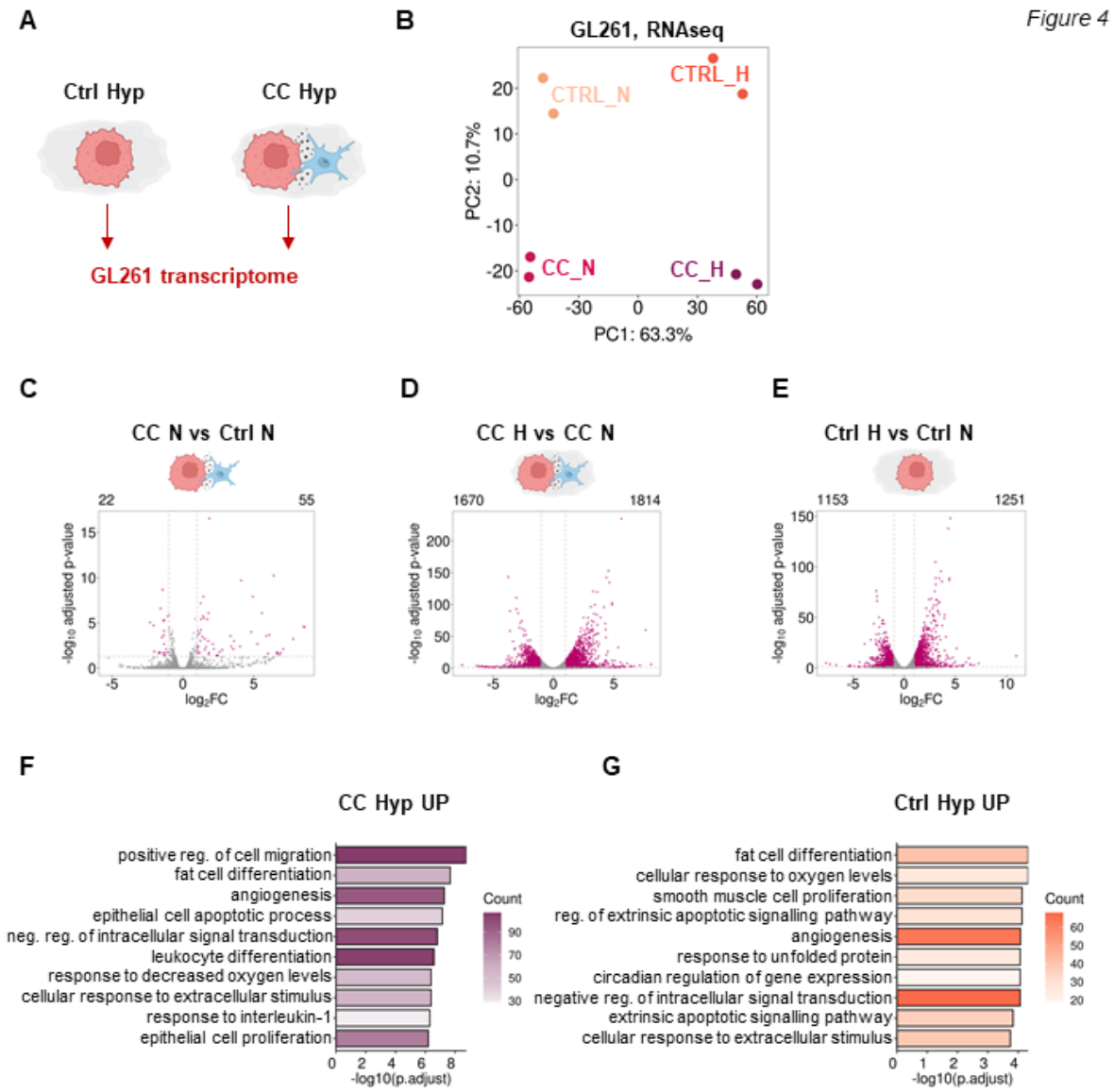
A
Ctrl Hyp
CC Hyp
GL261 transcriptome
B
GL261, RNAseq
CTRL_H
CTRL_N
CC_N
CC_H
PC2: 10.7%
PC1: 63.3%
C
CC N vs Ctrl N
22
55
D
CC H vs CC N
1670
1814
E
Ctrl H vs Ctrl N
1153
1251
-log10 adjusted p-value
log2FC
F
CC Hyp UP
positive reg. of cell migration
fat cell differentiation
angiogenesis
epithelial cell apoptotic process
neg. reg. of intracellular signal transduction
leukocyte differentiation
response to decreased oxygen levels
cellular response to extracellular stimulus
response to interleukin-1
epithelial cell proliferation
Count
-log10(p.adjust)
G
Ctrl Hyp UP
fat cell differentiation
cellular response to oxygen levels
smooth muscle cell proliferation
reg. of extrinsic apoptotic signalling pathway
angiogenesis
response to unfolded protein
circadian regulation of gene expression
negative reg. of intracellular signal transduction
extrinsic apoptotic signalling pathway
cellular response to extracellular stimulus
Count
-log10(p.adjust)

Figure 5

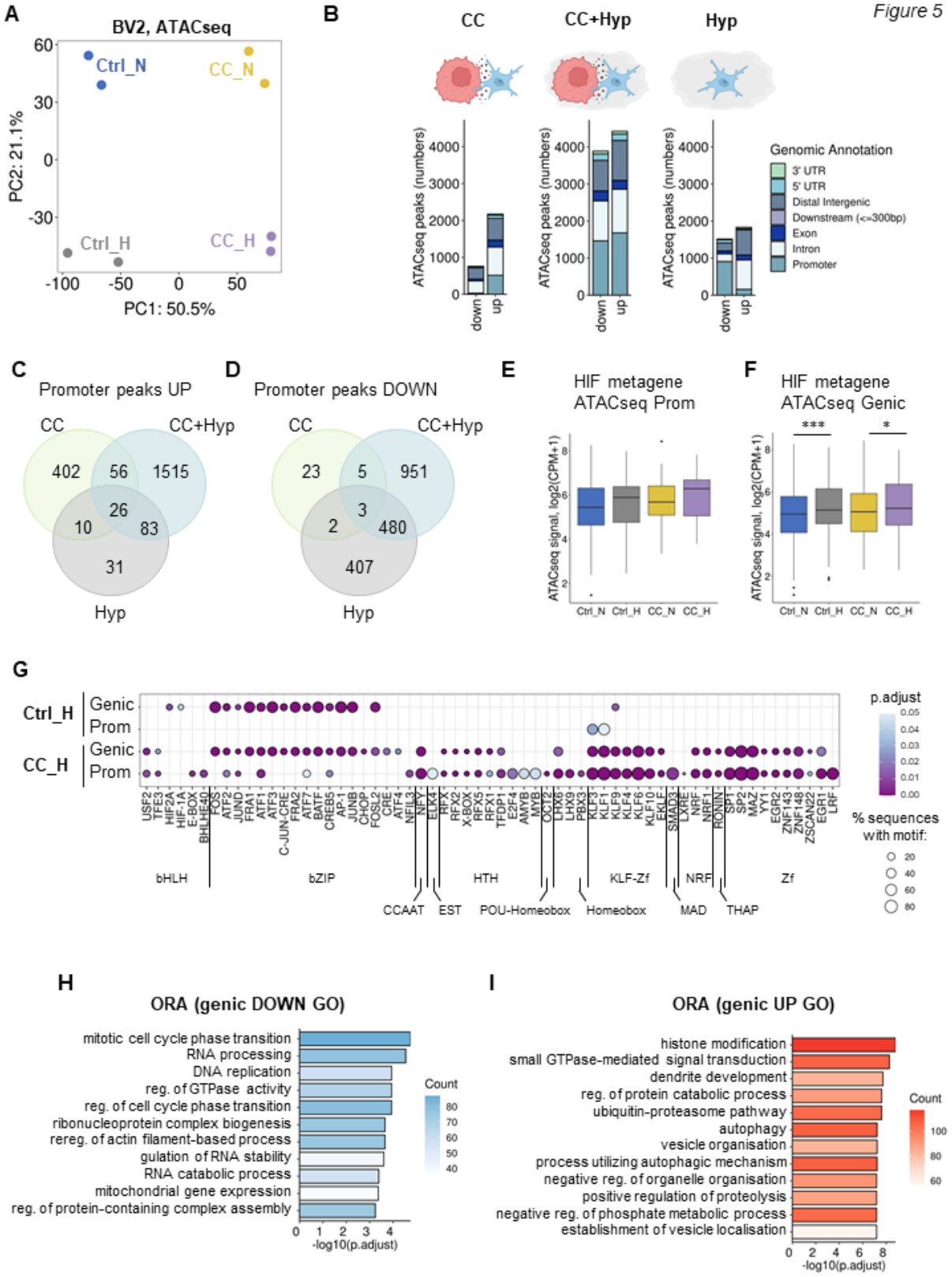
A
BV2, ATACseq
Ctrl_N
CC_N
Ctrl_H
CC_H
PC2: 21.1%
PC1: 50.5%
B
CC
CC+Hyp
Hyp
ATACseq peaks (numbers)
down
up
Genomic Annotation
3' UTR
5' UTR
Distal Intergenic
Downstream (<=300bp)
Exon
Intron
Promoter
C
Promoter peaks UP
CC
CC+Hyp
Hyp
402
56
1515
26
10
83
31
D
Promoter peaks DOWN
CC
CC+Hyp
Hyp
23
5
951
3
2
480
407
E
HIF metagene
ATACseq Prom
ATACseq signal, log2(CPM+1)
Ctrl_N
Ctrl_H
CC_N
CC_H
F
HIF metagene
ATACseq Genic
***
*
G
Ctrl_H
Genic
Prom
CC_H
Genic
Prom
p.adjust
% sequences with motif:
bHLH
bZIP
HTH
KLF-Zf
NRF
Zf
CCAAT
EST
POU-Homeobox
Homeobox
MAD
THAP
H
ORA (genic DOWN GO)
mitotic cell cycle phase transition
RNA processing
DNA replication
reg. of GTPase activity
reg. of cell cycle phase transition
ribonucleoprotein complex biogenesis
rereg. of actin filament-based process
gulation of RNA stability
RNA catabolic process
mitochondrial gene expression
reg. of protein-containing complex assembly
Count
-log10(p.adjust)
I
ORA (genic UP GO)
histone modification
small GTPase-mediated signal transduction
dendrite development
reg. of protein catabolic process
ubiquitin-proteasome pathway
autophagy
vesicle organisation
process utilizing autophagic mechanism
negative reg. of organelle organisation
positive regulation of proteolysis
negative reg. of phosphate metabolic process
establishment of vesicle localisation
Count
-log10(p.adjust)

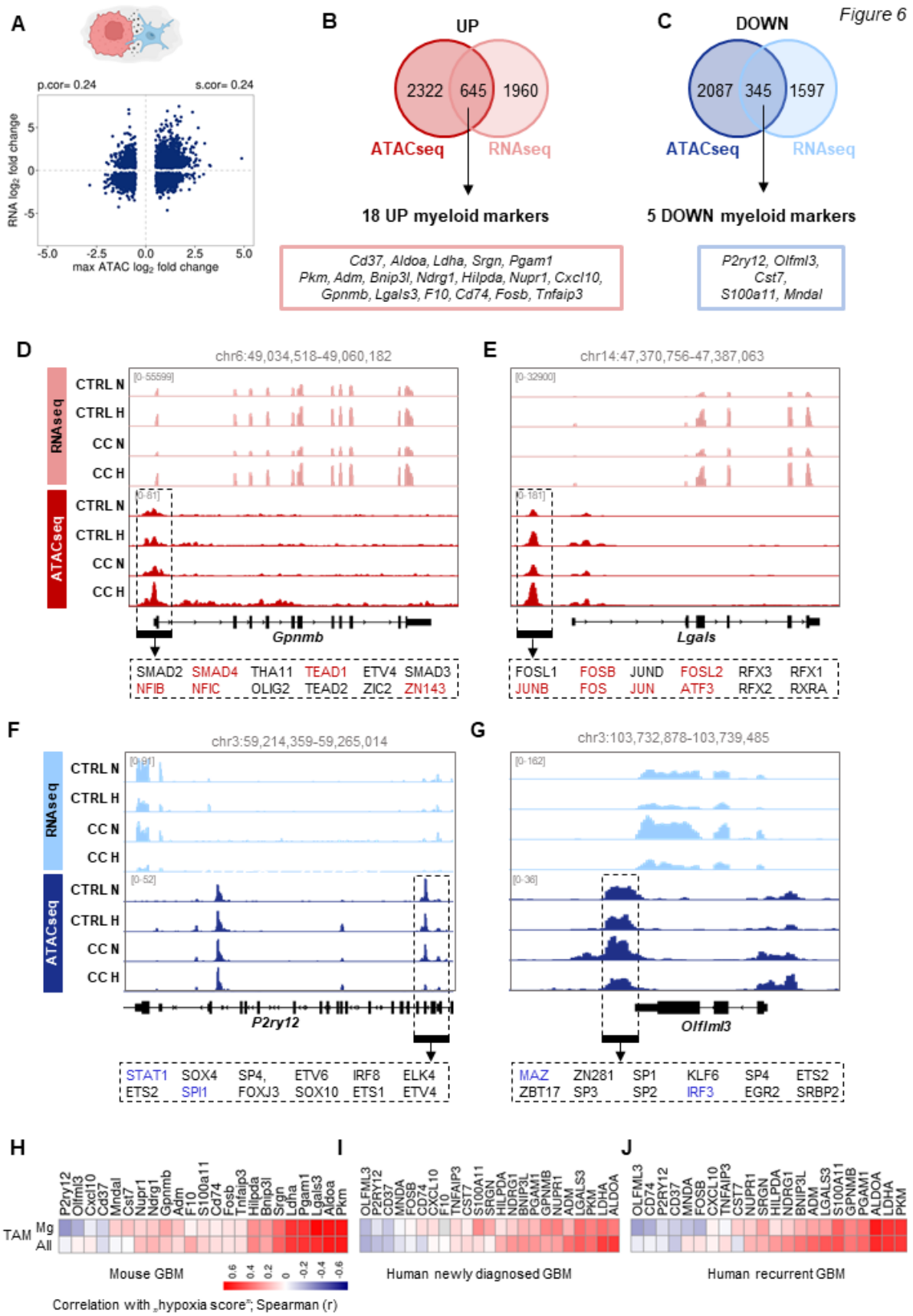
Figure 6
A
p.cor= 0.24
s.cor= 0.24
RNA log2 fold change
max ATAC log2 fold change
B
UP
2322
645
1960
ATACseq
RNAseq
18 UP myeloid markers
Cd37, Aldoa, Ldha, Srgn, Pgam1
Pkm, Adm, Bnip3l, Ndrg1, Hilpda, Nupr1, Cxcl10,
Gpnmb, Lgals3, F10, Cd74, Fosb, Tnfaip3
C
DOWN
2087
345
1597
ATACseq
RNAseq
5 DOWN myeloid markers
P2ry12, Olfml3,
Cst7,
S100a11, Mndal
D
chr6:49,034,518-49,060,182
RNAseq
ATACseq
CTRL N
CTRL H
CC N
CC H
Gpnmb
SMAD2 SMAD4 THA11 TEAD1 ETV4 SMAD3
NFIB NFIC OLIG2 TEAD2 ZIC2 ZN143
E
chr14:47,370,756-47,387,063
Lgals
FOSL1 FOSB JUND FOSL2 RFX3 RFX1
JUNB FOS JUN ATF3 RFX2 RXRA
F
chr3:59,214,359-59,265,014
P2ry12
STAT1 SOX4 SP4, ETV6 IRF8 ELK4
ETS2 SPI1 FOXJ3 SOX10 ETS1 ETV4
G
chr3:103,732,878-103,739,485
Olfml3
MAZ ZN281 SP1 KLF6 SP4 ETS2
ZBT17 SP3 SP2 IRF3 EGR2 SRBP2
H
TAM
Mg
All
Mouse GBM
I
Human newly diagnosed GBM
J
Human recurrent GBM
Correlation with „hypoxia score"; Spearman (r)